Greenland glacial history and local geodynamic consequences

L. Tarasov and W. Richard Peltier

Department of Physics, University of Toronto, Canada. E-mail: peltier@atmosp.physics.utoronto.ca

SUMMARY

Space–time reconstructions of the continental ice-sheets that existed at Last Glacial Maximum (LGM) have previously been produced using two entirely independent methodologies. One based upon the use of theoretical models of ice-sheet accumulation and flow and one based upon the geophysical inversion of relative sea level (RSL) histories from previously ice-covered regions. The analyses described in this paper demonstrate the significant advantages that derive from the simultaneous application of both methods to the particular case of Greenland. We thereby show that the ICE-4G reconstruction of the glaciation history of this region from LGM to present, which was based upon the geophysical inversion of RSL data alone, was reasonably accurate in the peripheral regions where RSL data were available but inaccurate in the interior of the ice-sheet, which was unconstrained by such information. We test the new model of Greenland glacial history determined by the simultaneous application of the constraints that derive from ice-sheet modelling and the geophysical inversion of RSL data by employing recently published geodetic inferences of mass-balance over the entire interior region of the ice sheet and of GPS measurements of vertical crustal motion. These observations, which were not employed to constrain the ice-sheet reconstruction, provide significant support for the new glacial history for Greenland that our analyses have led us to infer.

Key words: crustal deformation, glacial rebound, Greenland ice-sheet, isostasy, relative sea level.

1 INTRODUCTION

Reconstructions of deglaciation histories for regions that were ice-covered at Last Glacial Maximum (LGM) have been performed using two distinct methodologies. Models based on the geophysical inversion of observed relative sea level (RSL) histories (Peltier 1994, 1996, 1998) currently provide surface boundary conditions that are required for coupled atmosphere ocean general circulation model (GCM) based studies of past climates (e.g. Pinot *et al.* 1999; Vettoretti *et al.* 2000b). On the other hand, glaciological models that incorporate detailed descriptions of ice-sheet dynamics and which are forced by modelled or inferred climatologies have generally been used for process studies (Huybrechts *et al.* 1991; Huybrechts 1996; Calov & Hutter 1996; Ritz *et al.* 1997; Greve *et al.* 1998; Tarasov & Peltier 1997b, 1999) including recent investigations of the dynamical response of both Greenland and Antarctica to global warming (e.g. Huybrechts & de Wolde 1999; Greve 2000). Both of these approaches have advantages and disadvantages.

The reconstruction of the deglaciation history for a specific geographical region by inverting a set of local RSL histories suffers from a number of limitations. First, there is a degree of non-uniqueness due to the trade-off between the timing and the amount of load removed (a recent surface load variation is often indistinguishable from a larger variation of surface load that occurred earlier). Secondly, because of the inevitable sparse sampling of ice-covered regions by high quality ^{14}C dated RSL histories, and because of the inherently diffusive nature of the viscoelastic bedrock response to changes in ice load, the high frequency temporal and short wave-length spatial components of the deglaciation history are generally lost in the inversion. There is also significant sensitivity to the radial viscoelastic structure of the Earth that is required for the forward calculation of RSL histories. Finally, the geophysical inversion methodology is not constrained to deliver glaciologically plausible models of evolving ice-sheet form. All of these factors combine to restrict the quality of the reconstruction of the deglaciation process that one can produce using this method, even when detailed knowledge is available as to the time dependence of the ice-sheet margins based upon ^{14}C dated positions of terminal moraines. Geophysical reconstructions of the LGM to Holocene partial deglaciation of Greenland and Antarctica are especially difficult to obtain using this method given the localization of RSL observations to extra-marginal regions. On the other hand, RSL histories do provide very strong local constraints which any history of the deglaciation process must be able to satisfy. In relatively data rich regions such as those centred on Hudsons Bay and the Gulf of Bothnia, reasonably well constrained geophysical inversions are possible and have been produced (e.g. the ICE-3G model of Tushingham & Peltier 1991, 1992, 1994; and the ICE-4G follow-on model of Peltier 1991,

1994). Furthermore, RSL observations provide constraints on ice-sheet reconstructions that are independent of the often poorly constrained climatological inputs that are required in order to drive dynamical ice-sheet models and of the problematic specification of physical processes that occur at the ice–bedrock interface.

Dynamical ice-sheet models, on the other hand, deliver space–time variations of the ice-thickness field that are glaciologically self-consistent even though they are strongly sensitive to the usually poorly constrained climate forcings. With respect to the ice dynamics, basal processes which generally control fast ice flow are especially difficult to model given the small-scale processes that determine them. Boundary conditions such as those on geothermal heat flux and basal topography under existing ice-sheets are also known at best to a limited degree of accuracy. A series of recent ice-sheet model intercomparisons (Payne *et al.* 2000) in the context of the EISMINT project have validated the general consistency of the current suite of available thermomechanical models, though differences between their predictions are clearly evident in the details of the basal temperature fields for standard test cases.

The combination of these two methodologies for the reconstruction of ice-sheet histories through the explicit imposition of RSL constraints on dynamic ice-sheet models might reasonably be expected to provide a major improvement in the reconstruction of ice-sheet evolution. In particular, RSL observations are expected to provide a strong additional constraint that will significantly reduce the non-uniqueness of the unloading history due to the sensitivity of glaciological models to climate forcings and basal processes. Several recent RSL chronologies have been compiled for the main northern ice-sheets (Tushingham & Peltier 1991, 1992; Peltier 1994, 1998, 1999) yet the strong regional constraints that these chronologies offer have not been used by the ice-dynamics community to constrain their predictions. Since no serious attempt has yet been made to combine these two methodologies, it also remains unclear to what extent the imposition of such constraints can reduce the uncertainties in current glaciological models associated with their tuning degrees of freedom. Our primary goal in the present paper is to demonstrate that the combination of these methodologies provides a powerful means of reducing the uncertainties in the reconstruction.

The theoretical prediction of RSL histories, given a loading/unloading history for the continental ice-sheets, requires the specification of a detailed model of the radial variation of the viscoelastic structure of the solid Earth, including the thickness of the surface lithosphere. The viscosity of this outermost viscoelastic layer is so high that it is assumed to deform only elastically. As most recently reviewed in Peltier (1998), the radial viscoelastic structure may be quasi-independently inferred on the basis of the same RSL data used to reconstruct the deglaciation process when this is supplemented by additional information. The most difficult property of the radial viscoelastic structure to infer has proven to be the thickness of the surface lithosphere. Although this characteristic of the planet is clearly a strong function of location, it should be smallest near mid-ocean ridges and thickest, presumably, beneath mid-continental cratons. Previous models of the glacial isostatic adjustment process (recently reviewed in detail in Peltier 1998) have generally assumed lithospheric thicknesses of 120 km or more based upon the asymptotic thickness of the lithosphere beneath the oldest ocean floor originally inferred by Parsons & Sclater (1977). However, recent studies have argued for thicknesses as low as 65 km (Lambeck *et al.* 1998; Shennan *et al.* 2000). The reason why most past analyses of RSL data have not led to an unambiguous inference of lithospheric thickness is that most such analyses have been performed on data pertaining to the isostatic adjustment of regions loaded by ice-sheets of very large horizontal scale (such as Laurentia and Fennoscandia) and in such circumstances the response to unloading is not strongly sensitive to this feature of the model. The isostatic adjustment process does display high sensitivity to lithospheric thickness, however, in regions covered by ice-sheets of the scale that covered Scotland during the last glacial period. Through the recent re-analysis of the data from this region, Peltier *et al.* (2002) have been led to prefer a somewhat reduced lithospheric thickness of approximately 90 km for this region. This value is in accord with the most recent inferences of the thermal boundary layer thickness beneath the oldest ocean floor by DeLaughter *et al.* (1999) who obtained a value of 95 ± 10 km. In the analyses of the isostatic adjustment of Greenland to be discussed herein, the issue of lithospheric thickness will also be of primary concern.

As a test case with which to investigate the impact of the imposition of RSL constraints on a glaciological model, the Greenland ice-sheet is clearly the most suitable choice given: (1) it's current continued existence, (2) the availability of a significant number of coastal RSL histories, and (3) the strong dynamic constraint provided by the proximity of the ice margin to the shoreline and the narrowness of the adjacent continental shelf onto which LGM ice could have extended. Furthermore, the relatively small scale of Greenland as compared to the existing Antarctic ice-sheet will enable us to further explore the issue of lithospheric thickness. As mentioned above, larger scale load changes effectively probe more deeply into the Earth and are thereby more sensitive to the viscosity structure of the asthenosphere and deeper mantle than to the thickness of the lithosphere.

In this paper, we will compare the results of a previous inverse geophysical reconstruction for the deglaciation history of Greenland (as embodied in the ICE-4G model of Peltier 1994, 1996) with that delivered by a thermomechanical ice-sheet model. We will also investigate the extent to which the application of the constraint that the RSL response to the surface loading predicted using the glaciological model match RSL observations may further improve the quality of the reconstruction and allow us to further comment on the preferred value of the lithospheric thickness and/or shallow viscosity structure appropriate to this geographic region of the Earth. Analysis of computed RSL history sensitivities to ice-sheet model (ISM) parameter uncertainties will also provide a useful indication of the uncertainties in the local inferences of both Earth properties and the derived ice load chronology. Our analyses will conclude by providing a tuned ice-sheet model based glaciation history for Greenland that is both glaciologically self-consistent and that provides an excellent match to inferred RSL histories. As a means of testing the quality of this model, we will also present maps of the theoretically predicted vertical crustal motion for this region and for the current mass balance pattern over the ice-sheet interior. These predictions will be compared to the available observations and the excellent agreement between them will be construed to demonstrate the quality of the ice-sheet reconstruction that obtains when both geophysical and glaciological constraints are simultaneously applied.

2 MODEL DESCRIPTION

The complete ice dynamics model that will be employed for the analyses to be presented herein is composed of several interlinked components: (1) a recently updated thermomechanically coupled ice-sheet model, (2) a bed thermal model, (3) a basal sliding model, (4) mass-balance model using a positive degree-day approach (PDD) (Reeh 1989) but with a more physically-based melt factor and refreezing parameterization, (5) a viscoelastic bedrock model, (6) and finally, an ice 'age' tracking module.

2.1 Thermomechanical ice-sheet model

The original version of the thermomechanically coupled model has been fully described in Tarasov & Peltier (1999). Briefly, the model computes the flow of ice over the landscape using the vertically integrated continuity equation for ice mass in the form:

$$\frac{\partial H}{\partial t} = -\nabla_h \cdot \int_{z_b}^{h} \mathbf{V}(z)\, dz + G(\mathbf{r}, T),$$ (1)

in which H is the ice thickness and G is the surface and basal mass-balance (i.e. surface accumulation less surface and basal ablation and calving). Horizontal ice velocity $\mathbf{V}(z)$ is determined in the shallow ice approximation using the standard Glen flow law for the ice rheology, as:

$$\mathbf{V}(z) = \mathbf{V}_b - 2(\rho_i g)^n \{\nabla_h(h) \cdot \nabla_h(h)\}^{(n-1)/2} \nabla_h(h) \int_{z_b}^{z} A(T^*(z'))(h - z')^n\, dz'.$$ (2)

Here subscript b refers to the bedrock surface, h is the ice surface elevation above sea level, ρ_i is the density of ice, g is the acceleration due to gravity, and n is the flow law exponent ($=3$). The temperature dependent flow coefficient $A(T)$ is given by

$$A(T) = f(age)B \exp\left[-Q\left/\left(R_{\text{gas}} T^{\#}\right)\right.\right],$$ (3)

in which $f(age)$ is the flow law enhancement factor and $T^{\#}(z)$ is the temperature of the ice in degrees Kelvin, corrected for the pressure melting point. For surface elevation $h(x, y)$, $T^{\#}$ is given by $T_{\text{ice}}(z) - (h - z) \cdot 8.7 \times 10^{-4}$ K m^{-1}. The flow parameter B and activation energy Q are given by

$$B = \begin{cases} 1.14 \times 10^{-5}\,\text{Pa}^{-3}\,\text{yr}^{-1},\ Q = 60\,\text{kJ mol}^{-1},\quad T^{\#} < 263.15\,\text{K}, \\ 5.47 \times 10^{10}\,\text{Pa}^{-3}\,\text{yr}^{-1},\ Q = 139\,\text{kJ mol}^{-1},\quad T^{\#} > 263.15\,\text{K} \end{cases}$$ (4)

as per the EISMINT II specifications (http://www.esf.org/eismint; also Ritz *et al.* in preparation).

Recently, it has become rather unclear as to whether in fact the grain-size independent Glen flow law is appropriate for analyses of the flow of continent-scale ice-sheets (Peltier 1998; Peltier *et al.* 2000; Cuffey *et al.* 2000; Montagnat & Duval 2000). This issue is not, however, of primary concern for present purposes and so will not be discussed further. An enhancement factor of 3–5 to the standard Glen flow law has generally been found to be necessary in fitting ice-sheet models to Greenland observations. There are at least two reasons for this. First, previous studies have shown that increased model resolution requires decreased flow enhancement factors (Tarasov & Peltier 1997b) due to better numerical representation of the ice deformation. Second and more importantly, the standard isotropic Glen flow law, as employed in most current models, is based largely on extrapolations from a limited number of laboratory experiments (Paterson 1994) and it does not take into account several effects which are known to be important such as the development of anisotropic fabrics and changes in grain size (Jacka & Jun 1994; Goldsby & Kohlstedt 1997; Peltier 1998; Peltier *et al.* 2000). Observations from boreholes on Greenland for instance indicate a factor 2–10 enhancement of the flow law for older Wisconsinan ice relative to Holocene ice (Dahl-Jensen & Gundestrup 1987; Thorsteinsson *et al.* 1999) that is believed to be primarily due to the higher concentrations of impurities in Wisconsinan ice and/or the smaller ice crystal size. For the purposes of the present study, the flow enhancement parameter for older ice (i.e. older than Holocene) was set to 5.1 in order to achieve a close match to the present day surface elevation of the ice-sheet. f is reduced by a factor of 2.5 for Holocene ice in accord with the survey of Paterson (1991).

Determination of the ice temperature field (T) with the model takes into account both the full 3-D advection of heat but, as required by scaling arguments, only the vertical component of its diffusion. The advection-diffusion equation that must be solved simultaneously with the evolution eq. (1) is thus:

$$\rho_i c_i(T)\frac{\partial T}{\partial t} = \frac{\partial}{\partial z}\left\{k_i(T)\frac{dT}{dz}\right\} - \rho_i c_i(T)\mathbf{V} \cdot \nabla T + Q_d$$ (5)

Values assumed for the specific heat capacity of ice $c_i(T)$, its thermal conductivity $k_i(T)$, and other model parameters are listed in Table 1. A source term for heating due to deformation work Q_d is also included. Heating due to sliding, on the other hand, is accounted for in the basal thermal boundary conditions as discussed in Tarasov & Peltier (1999). Residual heat beyond that required to elevate the ice layer temperature to the pressure melting point is assumed to contribute to basal melting. Numerical discretization of the governing partial differential equation is carried out using a control-volume approach so as to ensure flux conservation, as discussed in Patankar (1980). The thermodynamic solver is fully coupled to the ice dynamics module, and includes 65 levels in the vertical. It is also implicitly coupled to a 5 level thermodynamic (vertical heat diffusion only) bedrock model that spans a depth of two kilometres. The geothermal heat flux employed for the analyses herein is from a new map which is described in Tarasov and Peltier (2002).

Table 1. Model parameters.

Definition	Parameter	Value
Earth radius	r_e	6370 km
Earth mass	m_e	5.976×10^{24} kg
Latent heat of fusion	L	3.35×10^5 J kg^{-1}
Ice density	ρ_i	910 kg m^{-3}
Ice specific heat capacity	$c_i(T)$	$(152.5 + 7.122\,T)$ J kg^{-1} K^{-1}
Ice thermal conductivity	$k_i(T)$	$9.828 \exp(-0.0057\,T)$ W m^{-1} K^{-1}
Bedrock density	ρ_b	3300 kg m^{-3}
Bedrock specific heat capacity	c_b	1000 J kg^{-1}°C^{-1}
Bedrock thermal conductivity	k_b	3 W m^{-1}°C^{-1}
Standard deviation, PDD model	σ	5.2°C
Standard deviation, accumulation model	σ_p	$\sigma - 1.$°C
Number of ice thermodynamic levels	nz_i	65
Number of bed thermodynamic levels	nz_b	5
Weertman sliding law rate factor	k_s	1.8×10^{-10} Pa^{-3} m^2 yr^{-1}

We have also incorporated an age module into the thermodynamic solver (required for determination of the age dependent flow coefficient f). We simply define a passive tracer Df, which is the date of formation of each ice parcel, and transport it through the ice with the boundary condition of $Df(\text{surface}) = \text{current time}$:

$$\frac{\partial Df}{\partial t} = -\mathbf{V} \cdot \nabla Df \tag{6}$$

A number of important numerical changes have also been made to the ice-sheet and thermodynamics models (as compared to those employed in Tarasov & Peltier 1997a, 1999) in order to improve ice mass and heat flux conservation under conditions of fast flow, namely:

(i) The linear matrix inversion involved in solving the ice dynamics equation has been made fully 2-D using Jacobi preconditioning with bi-conjugate gradient squared acceleration. We now employ the NSPCG software package (Kincaid *et al.* 1989) (available from the NETLIB web site, http://www.netlib.org/). Notably, this numerical methodology reduces run-time compared to the alternating direction implicit method with tri-diagonal solver that was previously employed. The package also allows the choice of numerous preconditioners. However, we have found that the simplest preconditioner, namely Jacobi, was the most efficient. Furthermore, the use of more advanced preconditioners did not enhance the numerical stability of the dynamic core of the model.

(ii) Mass fluxes are now properly accounted for in limiting ablation so as to prevent the occurrence of negative ice. (In earlier versions of the model, to avoid negative ice, ablation was limited to the amount of ice in the grid cell that could be melted in one time step. Now, ice flux into the grid-cell is also taken into account.)

(iii) The thermodynamic solver now uses the power-law scheme of Patankar (1980) for the discretization of the vertical advection-diffusion equation.

(iv) The computation of the temperature dependent flow coefficient now uses full upwinding.

(v) The iteration scheme for the solution of the non-linear ice dynamics equation now uses a series of relaxation factors to improve convergence: 0.82 for the first iteration, 1.0 (i.e. no relaxation) for the second, 0.75 for the third, and then 0.8 for the remainder.

(vi) A 2nd-order 5-point treatment (Payne & Dongelmans 1997) is now used to reduce artificial diffusion in the representation of horizontal heat advection. This improves the degree of radial symmetry of the solutions obtained in the ice block tests.

(vii) The analytical cancellations in the computation of the relative vertical velocity first mentioned by Ritz *et al.* (1997) are now also included. This results in an approximately 4 per cent decrease in model runtime and further improved radial symmetry in the ice block tests.

In order to provide a brief summary of the collective impact of these changes, we compare results for experiment A of the EISMINT II 'ice block' intercomparison (Payne *et al.* 2000) (Table 2) for a series of model refinements. 'Old' is the model that we previously submitted to the ice-sheet model intercomparison (Payne *et al.* 2000). Model 'Nh1' is the new model (modifications 1 to 5 above) but with O(1) horizontal advection as per Patankar (1980). These major changes have a relatively small impact as ice volume is decreased by only 1 per cent and the maximum ice thickness increases by only 23 m. The increase in horizontal area is purely the result of modification 4. The previously employed partial upwinding resulted in colder margins and thereby weaker marginal flux. Nh2 incorporates the second order horizontal advection scheme (modification 5) as per Payne & Dongelmans (1997), while Nh2P use a slight modification of this scheme in order to better conform to the logic of Patankar (1980), the main impact of which is a decrease in peak ice thickness of 15 m.

The final model version that is utilized for the following analyses (addition of modification 7) is 'Nh2Pw'. Overall, a significant change in numerics has brought only small changes to output ice statistics for the ice block tests, illustrating the general robustness of the model, at least for simple flow conditions. In comparison with the EISMINT II mean, our new model has 2.5 per cent more ice volume and 1 per cent thicker ice at the peak. The maximum ice thickness (and therefore also volume) tends to be somewhat high as most models in the intercomparison employ a non-conservative flux discretization scheme for the ice dynamics that is numerically more stable (Hindmarsh & Payne 1996), while our model computes all fluxes at cell interfaces in a fully conservative manner. The changes to our model have, more significantly, increased

Table 2. Comparison of ice block simulations. Nh∗ versions are all with the updated numeric scheme with various heat advection schemes as detailed in the text. 'Old' is the model previously submitted to the EISMINT II intercomparison (Payne *et al.* 2000). The EISMINT I and 'isothermal' values are for isothermal ice dynamics. The 'isothermal' model also uses the new Nh2Pw numerics but with only passive coupling of the thermodynamic module to the ice dynamics.

	Volume 10^{15} m^3	Area 10^{12} m^2	Basal melt area fraction	Maximum thickness m	Basal T at center K
Nh2Pw, new vert. advection	2.181	1.031	0.706	3724	255.92
Nh2P, Patankar horiz. advect.	2.181	1.031	0.706	3724	255.89
Nh2, O(2) horiz. advection	2.184	1.031	0.704	3739	255.92
Nh1, O(1) horiz. advection	2.174	1.031	0.701	3729	255.90
Old:	2.202	1.011	0.700	3706	256.26
EISMINT II Mean:	2.128	1.034	0.718	3688	255.605
EISMINT II Range:	0.145	0.086	0.290	96.7	2.929
Isothermal	1.973	1.013		3001	258.37
EISMINT I, Type I Mean:				2997.5 ± 7.4	257.11

its stability and improved the radial symmetry of the basal temperature maps delivered by the standard experiments of the intercomparison project (not shown).

Although the dynamics associated with basal sliding have small scale spatial-dependencies, especially pertaining to basal hydrology and land surface type, the absence of a sufficiently accurate representation of the sliding process necessitates the use of highly simplified models. We therefore continue to employ a simple Weertman-type sliding model (e.g. as in Huybrechts & de Wolde 1999) to compute the basal velocity $\mathbf{V}_b$ as a function of the basal shear stress σ_b and basal temperature T_b. For T_b near the pressure melting point (T_{pm}), this model computes $\mathbf{V}_b$ as:

$$\mathbf{V}_b = [-(T_{pm} - T_b)] \, k_s \, (\sigma_b)^2 \sigma_b / Z, \tag{7}$$

where $k_s = 1.8 \times 10^{-10}$ Pa^{-3} m^2 yr^{-1} . The factor Z is included to account for increased sliding when the base is below sea level (a crude attempt to account for the impact of basal hydrology) and is given by:

$$Z = \begin{cases} H & h \geq h_s, \\ \max(H + \rho_w(h - S)/\rho_i, 10 \text{ m}) & h < h_s, \end{cases} \tag{8}$$

where H is the ice thickness, h is the surface elevation, and S is the relative sea level. The basal velocity is set to zero for $T_b <$ (pressure melting point-1 K).

2.2 Viscoelastic bedrock model

In order to obtain the time-dependent surface elevation, required for the ice-dynamics, mass-balance, and surface temperature computations, the time-dependent bedrock elevation response to the changing surface ice and sea water loads must be determined. The bedrock response model is based on the use of the complete linear viscoelastic field theory for a Maxwell model of the Earth (Peltier 1974, 1976). The description of the radial surface deflection for an arbitrary applied surface load per unit area $L(\theta, \psi, t)$ is provided by the following space–time convolution:

$$R(\theta, \psi, t) = \int_{-\infty}^{t} \int \int_{\Omega} L(\theta', \psi', t') \Gamma(\gamma, t - t') \, d\Omega' \, dt' \tag{9}$$

where $\Gamma(\gamma, t - t')$ is the radial displacement Green function (Peltier 1974). The Green function can be represented in terms of surface load Love numbers h_l:

$$h_l(t) = h_l^E \delta(t) + \sum_{j=1}^{M} r_j^l \exp\left(-s_j^l t\right) \tag{10}$$

where h_l^E represents the instantaneous elastic component, and r_j^l are the viscous amplitudes with associated inverse relaxation time s_j^l that are required to represent the contribution to the response due to viscous relaxation. The full equation for the radial Green function in dimensional form is then

$$\Gamma(\gamma, t - t') = \frac{r_e}{m_e} \sum_{l=0}^{\infty} h_l(t - t') P_l(\cos \gamma) \tag{11}$$

The values that are used for the earth radius r_e and mass of the Earth m_e are given in Table 1.

Evaluation of the convolution integral (8) for the radial displacement response to a given history of surface loading is performed using the spectral methodology described in Peltier (1976). The spherical harmonic representation of the response delivered by the convolution integral

is truncated at degree and order 256 with a fixed time step of 100 yr and is thus asynchronously coupled to the ISM. Transient tests with a 50 yr time step for the coupling between the ice-sheet dynamics and the isostatically adjusting solid earth produced insignificant (<0.1 per cent discrepancy for ice volume and maximum surface elevation) differences. The ice-loading history in the convolution integral (9) is truncated 30 kyr prior to the current time step t. Load changes prior to $t - 30$ kyr are included as part of the $t - 30$ kyr contribution. As per the VM2 model of the radial viscoelastic structure, the elastic structure is that of PREM (Dziewonski & Anderson 1981), while the radial viscosity profile is taken to be represented by that of the VM2 model (Peltier 1996; Peltier & Jiang 1996). Based on the results of recent geophysical analyses of the glacial isostatic response of the British Isles (Peltier *et al.* 2002) and inferences of thermal boundary layer thicknesses beneath the oldest ocean floor (DeLaughter *et al.* 1999), we have chosen a base lithospheric thickness of 90 km. Given the limitations imposed by available computational resources, the bedrock model employs the eustatic approximation for the load component from all oceans. Although the ocean loading history may differ quite significantly from eustatic, previous investigations have found only limited discrepancies in the vicinity of the ice-sheet margins (Wu & Peltier 1982). This fact, in combination with the much larger load changes due to the ice-sheet itself, suggests that this simplification should have negligible impact on the ice-sheet dynamics. As such, with local ice thickness $H(\theta, \psi, t)$, the net surface load is given by

$$L(\theta, \psi, t) = \rho_i H(\theta, \psi, t) + \rho_w S_{\text{eus}}(\theta, \psi, t) \tag{12}$$

where ρ_i and ρ_w are respectively the densities of ice and sea water, and $S_{\text{eus}}(\theta, \psi, t)$ is the incremental eustatic thickness of the water column. It is extremely important to understand, however, that the theoretical predictions of RSL history that are employed to compare with the observations from coastal Greenland locations are computed off-line of the coupled ice dynamics bedrock model using the full gravitationally-self-consistent sea level solver (which is also topographically self-consistent with respect to changing coastlines as discussed in Peltier (1994), and as reviewed most recently in Peltier (1998). For the off-line sea level computation, we use the ICE-4G chronology for ice loads beyond Greenland. No useful purpose would be served here by reviewing the detailed structure of the theory that has been developed to predict postglacial RSL histories.

2.3 Mass-balance model and climate forcing

As per the EISMINT II intercomparison, we will initially employ a climate forcing inferred from the δ^{18}O record at the summit of the Greenland ice-sheet (GRIP) (Dansgaard *et al.* 1993; World Data Center-A for Paleoclimatology 1997). By δ^{18}O we herein imply the concentration of the less abundant ^{18}O isotope to that of the more abundant ^{16}O isotope relative to the same ratio measured in Standard Mean Ocean Water (SMOW). However, following the logic of Cuffey (2000), we will adjust the δ^{18}O to temperature conversion so as to take into account the impact of contemporaneous elevation changes on the δ^{18}O ratio of the surface accumulation. Our representation of the large scale climate forcing ΔT_c, is then given by

$$\Delta T_c = \frac{\Delta \delta^{18}\text{O} - (\lambda_\delta \cdot \Delta h_G)}{\alpha_c}, \tag{13}$$

in which Δh_G is the change in (modelled) surface elevation relative to present day at the GRIP site, and $\lambda_\delta = -6.2$ mil km^{-1} is the observed isotopic lapse rate in central Greenland (Johnsen *et al.* 1989). α_c is the climatic isotopic sensitivity. Results from recent inverse modelling of temperature vs borehole depth (Cuffey *et al.* 1995; Cuffey & Clow 1997; Dahl-Jensen *et al.* 1998) and gas-phase isotopic composition (Severinghaus *et al.* 1998) suggest values for α_c in the range of 0.15 to 0.43 (Cuffey & Marshall 2000). Preliminary reconstructions of the present-day borehole temperature profiles using our model favour a value of approximately 0.31 for the glacial phase and a value of 0.36 for the Holocene (Tarasov & Peltier 2002). It should be clear on *a priori* grounds that the use of a single temperature time-series $\Delta T_c(t)$, deduced in this way, to drive the evolution of the surface mass-balance of the Greenland ice-sheet, will constitute a crude representation of the actual geographically varying climate history. In tuning the glaciological model to conform to the observed variations of RSL history at coastal locations, we will therefore make use of local modifications to the ice-core inferred temperature field to force changes to the modelled glacial history that are required to obtain good fits to the RSL data.

A positive degree-day (PDD) method (Tarasov & Peltier 1999) with a standard deviation of 5.2°C is used to compute the ablation component of the surface mass-balance. However, we have added a mean June/July/August temperature (T_{jja}) dependence to the PDD ablation factors γ for both ice and snow (in ice equivalent) in order to conform to the recent results of energy balance modelling for Qamanarssup sermia (southwestern Greenland) (Braithwaite 1995):

$$\gamma_{ice} = \begin{cases} 17.22 \text{ mm/PDD} & T_{jja} \leq -1°\text{C}, \\ 0.0067 * (10 - T_{jja})^3 + 8.3 \text{ mm/PDD} & -1°\text{C} < T_{jja} < 10°\text{C}, \\ 8.3 \text{ mm/PDD} & 10°\text{C} \leq T_{jja}, \end{cases} \tag{14}$$

and

$$\gamma_{snow} = \begin{cases} 2.65 \text{ mm/PDD} & T_{jja} \leq -1°\text{C}, \\ 0.15 * T_{jja} + 2.8 \text{ mm/PDD} & -1°\text{C} < T_{jja} < 10°\text{C}, \\ 4.3 \text{ mm/PDD} & 10°\text{C} \leq T_{jja}, \end{cases} \tag{15}$$

Ice melt and snow melt factors respectively decrease and increase with temperature to account for the changing mix of turbulent and radiative surface energy fluxes.

We have also added a more physically-based refreezing model (Pfeffer *et al.* 1991; Janssens & Huybrechts 2000) that includes both thermodynamic and pore trapping components. For a given yearly snow-melt M, snowfall P_s, and rainfall P_r, the amount of superimposed ice (refrozen snow melt and frozen rain) for each year is now assumed to be given by:

$$\begin{cases} \min[P_r + M, 2.2 * (P_s - M) - d * c_i/L * \min(T_{surf}, 0°C)] & M < P_s, \\ \min[P_r + M, d * c_i/L * \min(T_{surf}, 0°C)] & M > P_s, \end{cases} \tag{16}$$

with a 1 m active thermodynamic layer d, a capillary factor of 2.2 and all components computed in ice equivalent thicknesses. The remaining parameters are defined in Table 1.

As found using much more detailed energy balance ablation models (Van de Wal 1996), the new PDD ablation/refreeze model has the strongest ablation anomaly relative to standard PDD models for lower amounts of ablation (Fig. 1). However, due to the use of a PPD formalism, the new PPD model still under-represents ablation at numerous grid-points where there are few or no PDD's but where the energy balance model may still predict significant ablation. Furthermore, the new model still produces ablation greater than 2.5 m yr^{-1} at numerous Greenland grid-points, in contradistinction to the energy balance model analyses. This high-end bias effectively helps compensate for the relatively large grid size. Past analyses have already established the need for enhanced ablation when using large-scale ice-sheet models to account for grid-scale effects (Ritz *et al.* 1997).

Precipitation is determined using a surface temperature and slope dependent modification of the present day field. Specifically, the base monthly precipitation at time t, $P(t, x, y)$, is computed by multiplying a present day precipitation climatology, $P(0, x, y)$, by a factor which depends explicitly upon the change of mean monthly surface temperature from present day ($\Delta T(x, y)$ in degrees Celsius) as per:

$$P(t, x, y) = P(0, x, y) * F_s * \exp(\eta * \eta_{xy}(x, y) * \Delta T(x, y)) \tag{17}$$

with a base value of 0.062 for η, chosen so as to attain a good match to the inferred age profile in the GRIP borehole (Tarasov & Peltier 2002). The complexities of mid-latitude cyclone dynamics and orographic effects clearly call into question the validity of such a simple temperature dependence, especially in the more southern and coastal regions. Lacking a viable alternative, we incorporate the uncertainty of regional precipitation changes into an additional tuning degree of freedom, $\eta_{xy}(x, y)$, that may be employed to improve the match between model and observations. In an attempt to capture some of the influence of orography on the local precipitation, a slope-dependent factor, F_s, is also included in (17), which is taken to be represented by:

$$F_s = \left(1 - \frac{h}{4 \text{ km}}\right) * \frac{\|\nabla h(x, y, t)\| + 0.001}{\|\nabla h(\text{observ})\| + 0.001} + \frac{h}{4 \text{ km}} \tag{18}$$

which is based upon the representation employed by Ritz *et al.* (1997) but which includes an added weakening of the slope effect with elevation as is required to obtain better matches to the GRIP borehole temperature and age profiles and to the inferred accumulation history (Tarasov & Peltier 2002).

For the purpose of the analyses to be discussed herein we will employ a modern precipitation map for the field $P(0, x, y)$ in (17) that has been derived by inversion of a recently published digital accumulation map (Ohmura *et al.* 1991) for regions over 1500 m in elevation, together
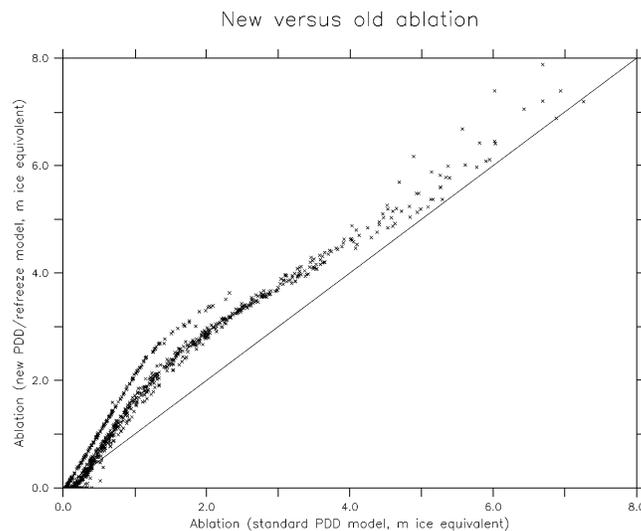

Figure 1. Comparison of the standard Positive Degree Day (PDD) surface mass-balance model in ice equivalent with the revised model using temperature dependent degree day coefficients. Points represent individual grid cells on the input topography with unmodified present-day climate forcing. See text for further discussion.
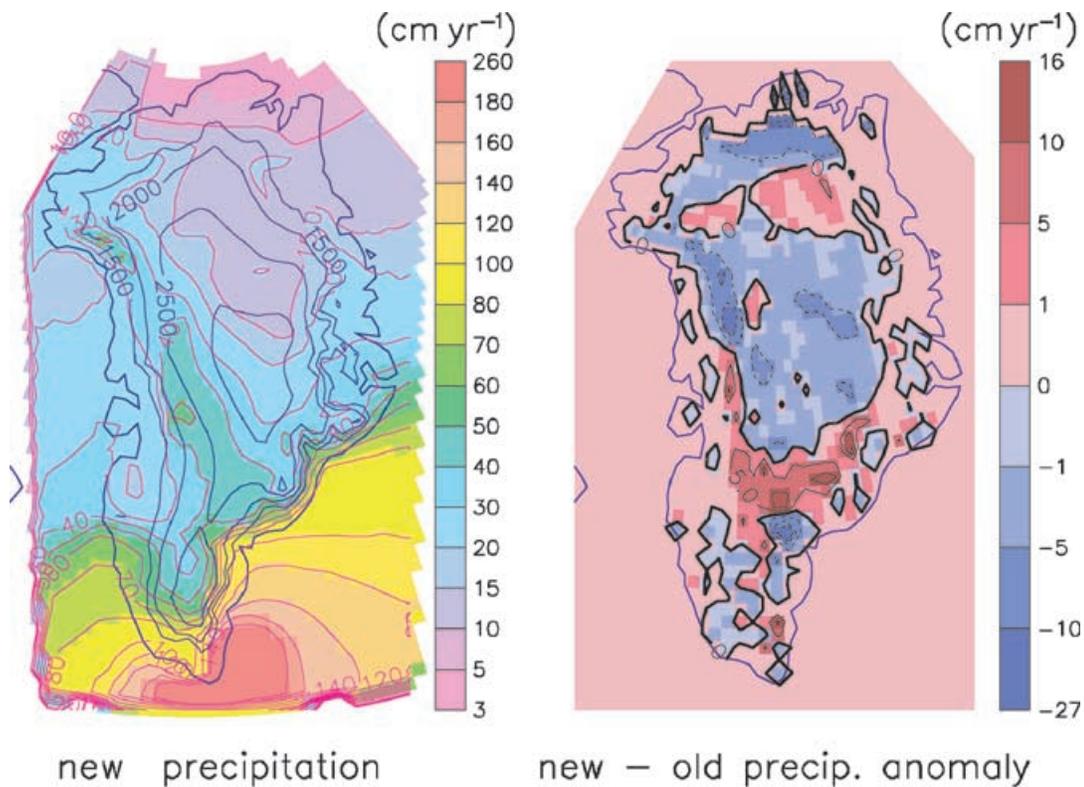
Figure 2. New present-day precipitation map (computed by inversion of the accumulation map of (Ohmura *et al.* 1991) with surface elevation contours from the revised topography of Bamber *et al.* (2001) and precipitation anomaly with respect to the previous map of Ohmura & Reeh (1991). Refer to text for details.

with an older precipitation map for lower elevation regions (Ohmura & Reeh 1991) (where sensitivity to the assumed surface temperature and ablation model brought the above inversion into question). Specifically, the higher elevation precipitation field was derived by the requirement that under the accumulation model with present-day climate forcing and observed elevation, the required accumulation field is obtained. We have also imposed a precipitation reduction in the north-northeast sector (east of 60W and north of 80N) to improve the model fit to present day topography. The new precipitation map (Fig. 2) generally has less precipitation over the core of the ice-sheet, especially in the western sector. A region of increased precipitation also exists over the saddle region to the south. The area-weighted average precipitation for the new map is 34.2 cm yr^{-1} vs 35.1 cm yr^{-1} for the older map. Seasonal variability of the precipitation field is determined on the basis of the observational data set of Legates & Willmott (1990). Accumulation is also determined using a normal statistical model to compute the fraction of a monthly period characterized by temperatures below 2.0°C (Tarasov & Peltier 1999).

It is clear on the basis of observations that ice calving plays a key role in the mass-balance of the Greenland ice-sheet. However, calving is a process that is highly sensitive to small-scale physical influences, and is therefore very difficult to represent in a model having relatively low spatial resolution. We will employ a simple model in which the rate of calving is assumed to be proportional to the grid-box buoyancy of the marginal floating ice (with a default proportionality factor k_C of 0.5 m yr^{-1} per metre of buoyancy). We also impose the condition that calving is only allowed to occur when there exists an adjacent ice free deep-water grid-cell. In reality, calving and ice discharge are complicated processes sensitive to the small-scale geometry of the discharge basin, tidal ranges, ocean currents and regional temperatures. In fjords and narrow straits calved ice can back up, or even plug up the basin, and significantly reduce discharge into the free ocean. As such, we absorb, to some extent, these small-scale dependencies by treating k_C as a tuning parameter when required to obtain matches to the RSL observations.

The input basal and surface topography for Greenland (Fig. 3) (Letreguilly *et al.* 1991) has significant surface elevation discrepancies compared to more recent and more accurate maps (e.g. Schaeffer *et al.* 1999; Bamber *et al.* 2001). Unfortunately, no other maps with a co-validated bedrock map on the same grid were available when the analyses presented herein were undertaken. Comparisons of computed vs observed surface elevation anomalies will however be presented using the newer map of Bamber *et al.* (2001). Ocean bathymetry and a truncated version of Ellesmere Island topography were taken from the ETOP05 data set. Given the lack of available data sets for present day ice thickness on Ellesmere Island, we assume no initial ice over the island.

2.4 Model coupling

Model subcomponents are flexibly coupled. The ice-sheet model employs a variable time step (12.5 yr−0.390625 yr) as required to ensure convergence. Ice and bedrock temperatures are computed every 2 ice dynamic time-steps with a lower cut-off of 12.5 yr. Furthermore, the
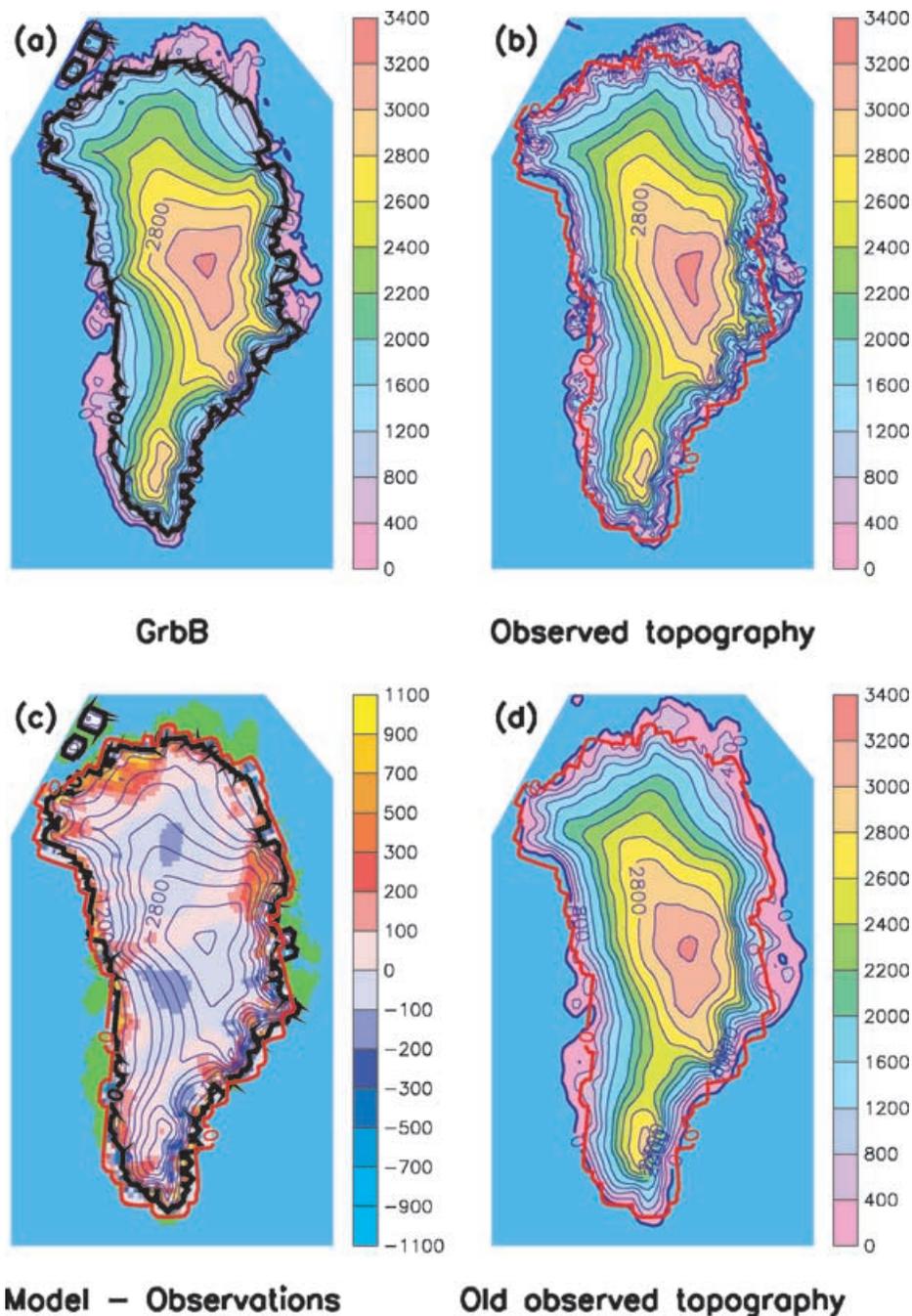
Figure 3. (a) Surface elevation using the fully tuned model GrB compared with (b) the observed topography (Bamber *et al.* 2001). Also shown is (c) the elevation difference between modelled (GrB) and observed surface topography and (d) the input Greenland topography from Letreguilly *et al.* (1991). The black contour is the modelled ice margin. The red contour denotes the observed ice margin.

ice thermodynamic/age solver incorporates nested time loops with interpolated input fields to meet linear stability requirements. Surface mass-balance is computed every 2–4 time-steps with a lower cut-off of 3.125 yr.

Simulations are initialized with the EISMINT II standard gridded basal topography and ice-sheet thickness field using −250 kyr climatic boundary conditions. For lack of an alternative, the bedrock is then assumed to have been in isostatic equilibrium with the observed present day gridded ice-sheet load. The model is first run to near equilibrium using accelerated thermal parameters for 110 kyr and then a full 250 kyr cycle is computed. The duration of the transient cycle was chosen so as to compensate for use of equilibrium initial conditions.

3 RSL OBSERVATIONS

The University of Toronto RSL database for Greenland consists of ^{14}C dated age–height pairs and geographic location for marine samples (mostly mollusk shells) compiled from a number of sources (Table 3). The ^{14}C age to calendar year conversion has been computed using the

Table 3. Sources for RSL observations for Greenland along with ^{14}C reservoir corrections (δR).

Label	Lat.	Long.	# of data	δR	Site name	Source
2001	81.66	−60.01	28	287 ± 70	Hall Land	England (1985), Dyke pers. comm.
2002	76.72	−73.12	5	287 ± 70	Carey Is.	Blake (1977), Dyke pers. comm.
2003	69.59	−53.88	59	−55 ± 106	Disko Is.	Rasch (1997)
2004	69.09	−51.02	88	−55 ± 106	Disko Bugt	Rasch (1997)
2005	66.65	−51.92	8	31 ± 52	O. Sondre Stromfjord	Ten Brink & Weidick (1974)
2006	66.54	−51.08	11	31 ± 52	I. Sondre Stromfjord	Ten Brink & Weidick (1974)
2007	64.43	−50.20	4	129 ± 84	Kapisigdlit Cw	Weidick (1972a,b)
2008	62.10	−49.55	6	129 ± 84	Nerutussoq Cw	Weidick (1972a,b)
2009	60.97	−46.65	1	129 ± 84	Julianehaab	Shottont & Williams (1974)
2010	72.00	−24.00	24	123 ± 80	Mesters Vig	Washburn & Syuiver (1962), Trautman & Wills (1963)
2011	72.25	−24.25	13	123 ± 80	Skeldal	Lasca (1966)
2012	80.55	−21.67	17	152 ± 33	K. Christian Land Ne	Weidick (1972a,b)
2013	82.15	−31.20	23	152 ± 33	J. Bronlund	Weidick (1972a,b)
2014	82.92	−24.25	6	152 ± 33	Peary Land	Weidick (1972a,b)
2015	83.08	−32.25	3	152 ± 33	F. E. Hyde Fd.	Weidick (1972a,b)
2016	83.60	−30.50	2	152 ± 33	Kaffeklubben O	Weidick (1972a,b)

Calib 4.2 software (based on Stuiver & Reimer 1993) using the intercepts method with σ confidence limits, Marine98 calibration (Stuiver *et al.* 1998) and ocean reservoir corrections (δR in Table 3) inferred from the Marine Reservoir Correction Database (http://depts.washington.edu/qil/marine/). RSL data-points have been coalesced so as to define RSL history at 16 sites whose geographic locations are shown on Fig. 4.
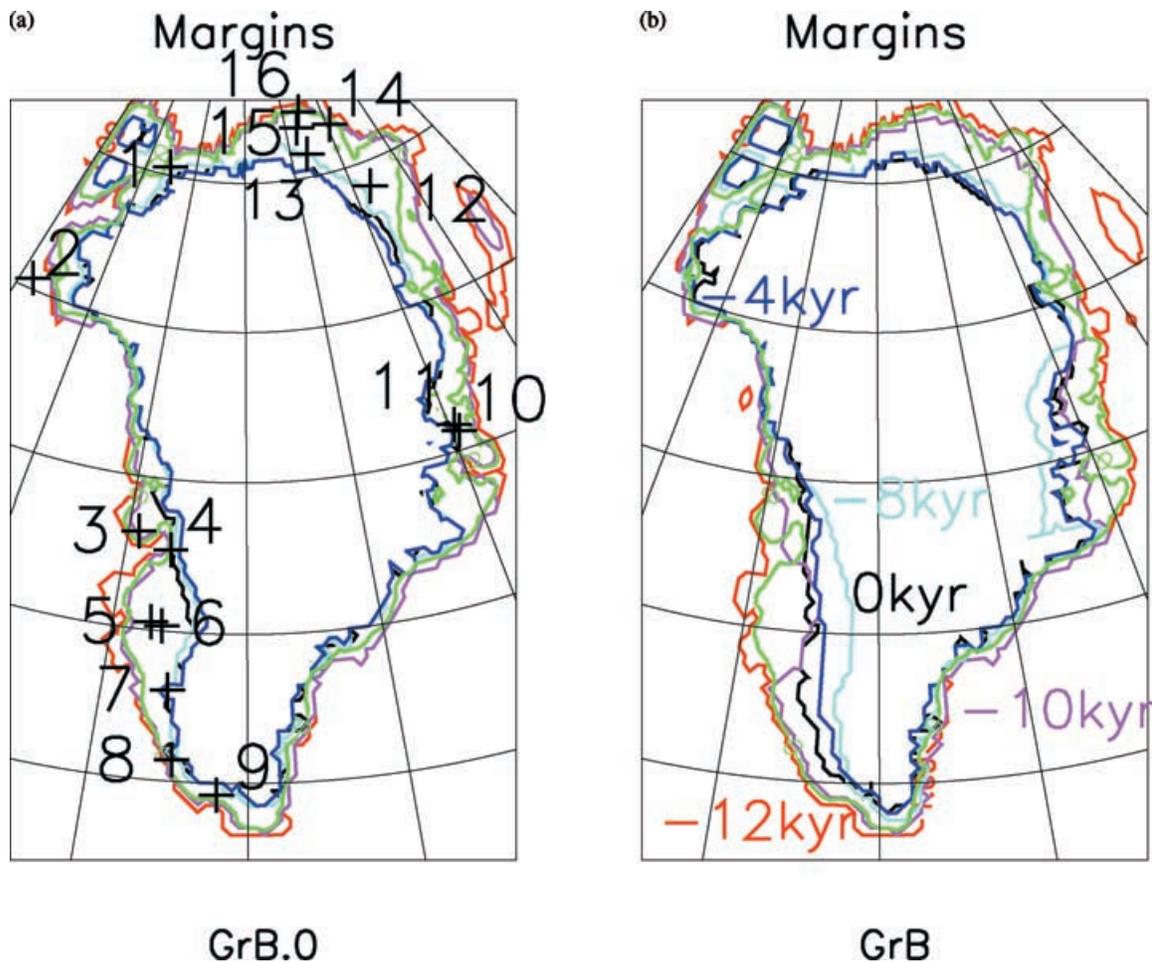

Figure 4. RSL site map and margin positions for the untuned (GrB.0) and fully tuned (GrB) models. Red margin is full late glacial extent at −12 kyr. Violet is −10 kyr margin. Light blue is Holocene minimum at −8 kyr. Dark blue is −4 kyr margin, black is present-day margin and green is present-day model coastline.

In inferring an RSL history from such data-sets, tides, waves, sediment consolidation, and bioturbation can disturb the physical location of the sample and thereby invalidate the age-height data-point. The sample selection process attempts to screen for these impacting factors. However, as will become evident, the data-point scatter for many sites makes definitive identification of an RSL envelope difficult. Given that the apparent scatter is strongest for those sites with the most data-points, it is clear that even sites with no apparent scatter and few data-points must also be interpreted with caution. The most important factor in interpreting data-points is the contemporaneous location of the sample source. The molluscs whose shells form the main marine sample set for the available data may live well below the sea surface. As such, the envelope defined by marine-based RSL data-points should generally be interpreted as representing some lower limit of the true RSL envelope.

4 RESULTS

Our new model of the Greenland glacial cycle is highly tuned to the Holocene period. Although some effort was also expended to ensure that the model provides a reasonable match to the present day observed topography of the Greenland ice-sheet, our primary tuning target was the set of inferred RSL histories from the University of Toronto RSL database discussed above. The model was also tuned to fit the GRIP borehole temperature and age profiles (Tarasov & Peltier 2002). The secondary target concerning the match to present day topography was given much less emphasis. As an initial test of the utility of the RSL constraints, model tuning was first carried out with no attention to any other possible constraints on the deglaciation chronology except for the Disko region where the considerable scatter of the data left the tuning target somewhat unclear. At this location further constraints on Holocene marine limits and time of crossover to below present day sea-levels were also employed (Rasch & Nielsen 1995).

4.1 Sensitivity to tuning parameters

A number of small-scale modifications to the climate forcing and calving model were required to obtain a match to inferred RSL histories. In order to illustrate the impact of these modifications on computed RSLs, we have produced a series of increasingly tuned model simulations. Model GrB.0 utilizes the global tuning parameters (flow enhancement, sliding parameter, accumulation parameter, α_c) along with the new heat flow map required by the fully tuned model to match ice-volume, topography, age-profile, and ice temperature constraints. GrB.0 does not incorporate any local tuning of calving, accumulation, and climate forcing used by the fully tuned model to match RSL observations. Model GrB.0 invokes only one regional adhoc modification to the climate forcing (represented by the single time-series $\Delta T_c(t)$ defined in 13) and none to the calving model. A linear increase in the strength of surface temperature forcing ($\Delta T(t)$) was imposed starting from latitude 72N to a maximum increase of 50 per cent at 62N. This was required to better match the computed Dye3 borehole temperature profile (Tarasov & Peltier 2002). Previous 1-D modelling analyses of the Dye3 ice core (Dahl-Jensen *et al.* 1998) also found the need for a 50 per cent increase in the surface temperature amplitude as compared to that inferred for the GRIP site. Given the proximity of this southernmost region of Greenland to the jet stream, which GCM analyses suggest to have been significantly displaced during glacial periods (e.g. Kutzbach & Guetter 1986; Fawcett *et al.* 1997), this increase in the strength of the regional temperature variation is quite plausible. Borehole temperature profiles from the Northern region of Greenland would be useful for constraining changes to the glacial climatic variability in that region.

Computed RSL chronologies for this model (long-dashed line in Fig. 5) illustrate the weak RSL response for all sites excepting those in the north-northeast (stations 12–16) which have excessive response, and for Sondre Stromfjord in the southwest. The general pattern of LGM to present day margin movement is one of near monotonic shrinkage from −12 kyr to −8 kyr with near negligible late Holocene re-advance (Fig. 4a). The ice-sheet area of model GrB.0 (Table 4) is slightly less than that observed, yet the volume of the simulated ice-sheet is approximately 9 per cent greater than observed. This model overestimation of present day ice volume is a feature in common with other models (e.g. Huybrechts & de Wolde 1999), and is likely due to a combination of effects such as those due to: errors in the gridded input surface and basal topography, grid-scale effects (Tarasov & Peltier 1997a), the simplicity of the imposed climate forcing and mass-balance model, poor resolution of ice stream and outlet glacier dynamics due to both the lack of accounting of longitudinal stresses and the limited grid-resolution, and the invalidity of the assumption of present-day isostatic equilibrium which was required for the initial model boundary conditions. Even with this ice volume excess, however, the root-mean-square error in surface topography over the ice-sheet, with respect to both old (input) and new topographic data sets, is, respectively, only 76 and 82 m.

Model GrB.C incorporates local reductions of the calving parameter for Nares strait between Greenland and Ellesmere Island (0.03 m yr^{-1} for the southern part, 0.01 m yr^{-1} for the northern half of the strait), for the Disko area (0.07 m yr^{-1}), for the Sondre Stromfjord area (0.1 m yr^{-1}), and for the region around the eastern stations (Mesters Vig and Skeldal, 0.03 m yr^{-1}). These calving modifications alone result in much increased RSL response for: Hall Land, Disko, Mesters Vig, and Skeldal (medium-dashed line in Fig. 5).

Model GrB.CP invokes the addition of further regional modifications to the precipitation dependence (η_{xy} in eq. 17) on assumed changes in surface temperature. η_{xy} was linearly decreased from the value of unity to a value of $1/2$ in the region from 68 to 60 degrees north for $dT < 0$C) (relative to present day). This was necessary both to better match the Dye3 borehole temperature profile (Tarasov & Peltier 2002) and to provide more late glacial ice loading in the region as indicated by the misfits to the RSL records from Kapisigdlit and Nerutussoq Cw for model GrB.0. This modification largely offsets the impact on the amount of precipitation due to the regional linear increase in surface temperature forcing that is imposed on all models to improve the match with the temperature profile from the Dye3 borehole (Tarasov & Peltier 2002). The direct effect of this reduction in the sensitivity of precipitation to the variation of surface temperature is a rather small increase in the RSL response at the southerly sites (07–09, short-dashed line, Fig. 5). However, the additional ice accumulation in the south
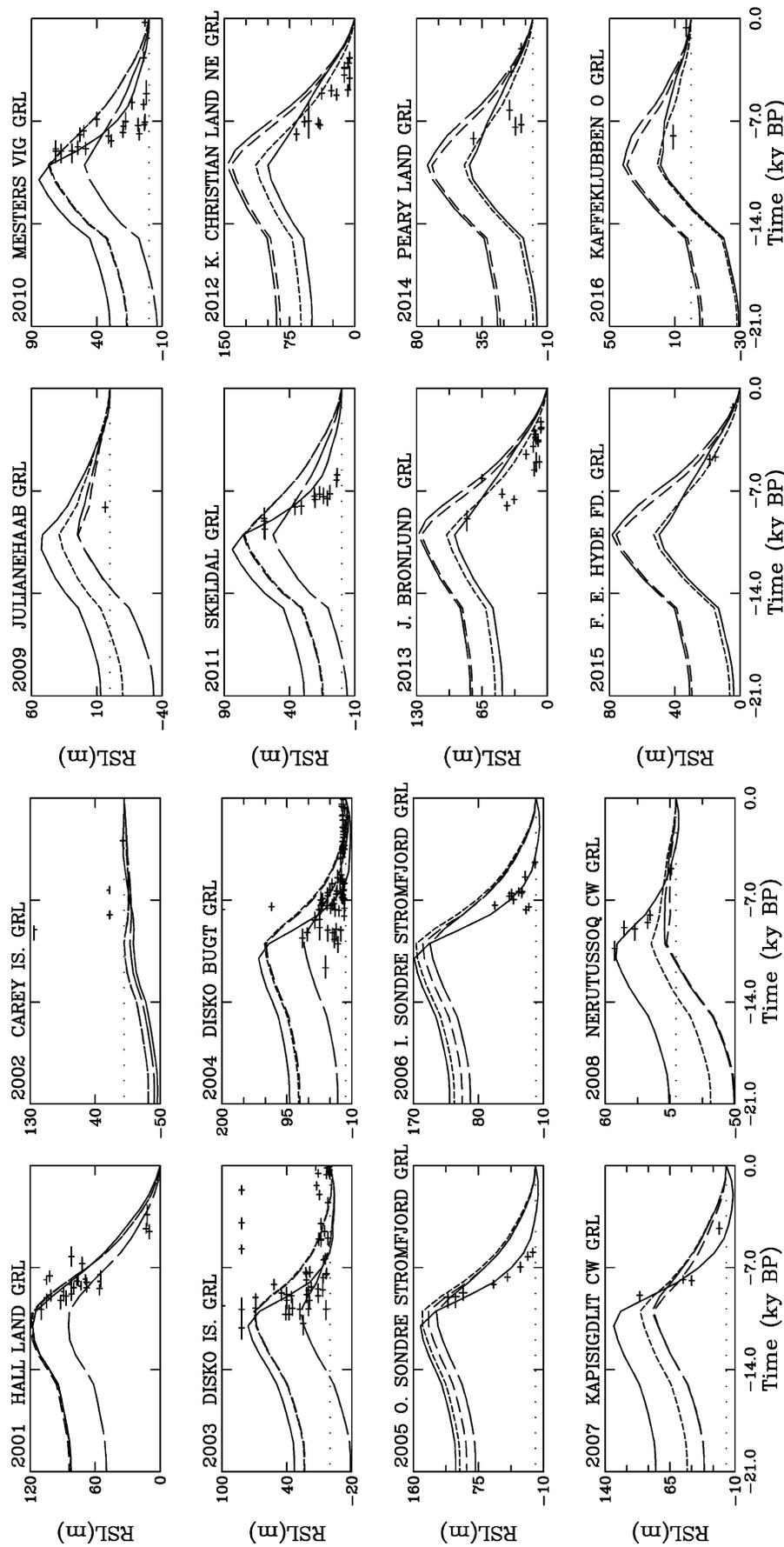
Figure 5. RSL data-points and computed chronologies for the bare model with unadjusted calving and precipitation (GrB.0 long-dashed), and for the models with: adjusted calving (GrB.C medium dashed), adjusted calving and precipitation sensitivity (GrB.CP short dashed), and fully tuned (GrB solid line). Refer to text and appendix for details of model tuning.

Table 4. Comparison of Greenland Ice-Sheet Simulations. σ is the rms difference with respect to input ice surface topography (Letreguilly *et al.* 1991) and σ_K is with respect to the newer observational topography of Bamber *et al.* (2001). The mass-balance is the average value for the last 100 yr of model time.

	Obs.	Grid. obs	GrB.0	GrB.C	GrB.CP	GrB	GrBb	GrB.A66
Vol. 10^{15} m^3	2.828	2.847	3.07	3.08	3.09	3.08	3.02	3.07
Mass-bal. km^3 yr^{-1}			64	64	43	2	4	−6
Area 10^{12} m^2	1.75	1.748	1.70	1.71	1.72	1.71	1.68	1.71
σ m		0.0	75.9	75.1	76.0	70.0	61.6	69.5
σ_K m		45.56	82.1	81.4	82.1	79.0	70.3	79.1
Max. elev. m	3230	3254	3258	3251	3253	3245	3249	3246
H(GRIP) m	3029	2951	2987	2979	2981	2963	2959	2964

was important for allowing more load to be removed in the fully tuned model when modifications were added to the Holocene temperature forcing. The parameter η was also increased by a factor of 1.5 to 2 in the north-northeast (for colder than present temperatures only) to reduce the RSL response there.

These regional modifications to η and to the calving parameter account for the improvement in the RSL fits achieved with the fully tuned model (GrB, solid line in Fig. 5) at the northeastern RSL sites (12–16). However the remaining sites require significant modifications to the local Holocene temperature forcing to provide reasonable matches to observations. The physical justification of such an ad-hoc modification to the climate forcing can be ascribed to two key factors. First, the assumption of a model for climate forcing based on a single temperature proxy record from summit, Greenland, is of questionable validity for application in the near-coastal climate-sensitive ablation zones, especially since analyses based on stacked isotopic records covering the last few centuries reveal only limited correlation with similar records from the Summit region (White *et al.* 1997). Secondly, the crude representation of basal processes and the lack of explicit ice stream and outlet glacier dynamics in the model also imply a significant under-representation of the meso-scale dynamic response of the ice sheet to the climate forcing.

Calving processes are also poorly represented in the model, but consideration of the RSL sensitivity results in Fig. 5 indicate that this is an unlikely rational for the adhoc Holocene temperature forcing adjustment. The impact of this temperature forcing adjustment is primarily to speed up and adjust the timing of the RSL response. The only exception to this is for the Kapisigdlit and Nerutussoq sites to the south-southwest where limited shelf extent limits the sensitivity to the calving parametrization. Regional calving and precipitation sensitivity parameter variations on the other hand have little impact on the timing of the RSL response (Fig. 5). This is partly due to the fact that calving ceases to be a factor once the ice-margin is terrestrial and Holocene temperature forcing adjustments were largely required in regions where the ice margin was significantly inland by −8 kyr (Fig. 9). Instead, calving primarily controls RSL amplitude for all sites on the west side of Greenland as well as Mesters Vig and Skeldal to the east, while precipitation sensitivity adjustments are used to tune down the amplitude of emergence predicted for northeastern RSL sites. This difference in RSL response to tuning parameters therefore strongly suggests that the adhoc Holocene temperature forcing is not significantly accounting for the simplicity of the calving model.

The details of these various modifications to the time-dependent surface temperature forcing (ΔT_{adj}) are provided in the appendix and the related Table A1. Briefly, these involve local increases in surface temperature which are linearly ramped up from approximately the end of the Younger Dryas period to a maximum strength around −9 kyr ranging from 3 to 10°C depending on location. ΔT_{adj} is thereafter decreased after 8 kyr to a steady value by −5 kyr that ranges from 3.2 to −2.0°C. These modifications therefore have no direct impact on late Holocene climate variability but are in accord with expectations based upon orbitally induced variations in insolation through the early Holocene (e.g. see Vettoretti *et al.* 2000a). A constant −3.0°C regional cooling to the northeast (i.e. in the vicinity of Thule) is also imposed from −11.5 kyr onwards in order to obtain an improved margin extent in that region.

Overall, the fully tuned model GrB provides an excellent match to the RSL records even though the scatter evident in these records at many of the sites precludes definitive identification of the RSL envelope. Especially problematic and interesting are the Disko and Mesters Vig sites. Recent studies based upon the use of ^{14}C measurements in peat horizons (which tend to provide a good upper bound for RSL data-points) argue for below present late Holocene RSLs for both Disko Island (Rasch & Nielsen 1995) and Disko Bugt (Rasch 2000). For this reason, model GrB was tuned for a near −5 kyr crossover to lower than present relative sea levels at Disko Island, close to the −4.7 kyr estimate of Rasch & Nielsen (1995). The 76 m model marine limit for Disko Island was tuned to be in approximate accord with the general pattern of Holocene marine limit observations for the island which these authors have also discussed.

The topography and local ice dynamics in regions such as Disko Bugt make it clear that local tuning is unavoidable for current state-of-the-art ice-sheet models. The 0.5 by 0.25 degree longitude/latitude grid resolution is at the limit that is reasonable in the context of analyses performed with an ice dynamics model based upon the shallow ice approximation. Even at this resolution, Disko Island appears as a peninsula on the gridded topography. Another complicating factor for the region is the presence of fast ice flow. Disko Bugt is located at the mouth of Jakobshavns Isfjord which drains Jakobshavns Isbrae, an ice stream about 6 km wide, 90 km long and for which continuous surface velocities up to 7 km yr^{-1} have been recorded (Echelmeyer *et al.* 1991). The model also delivers a large scale fast flow in the region (Fig. 6) though with much lower velocities and weaker cross-flow gradients due both to the grid resolution and to the lack of explicit ice-stream mechanics. Recent analyses for Antarctica (Ritz *et al.* 2001) have clearly illustrated the increased sensitivity of the ice-sheet response to climate, and especially sea level, forcing when explicit ice-stream mechanics are included. As such, it is likely that the regional modifications to Holocene temperature forcing imposed herein are at least partly accounting for the lack of a detailed representation of ice streams in the model.
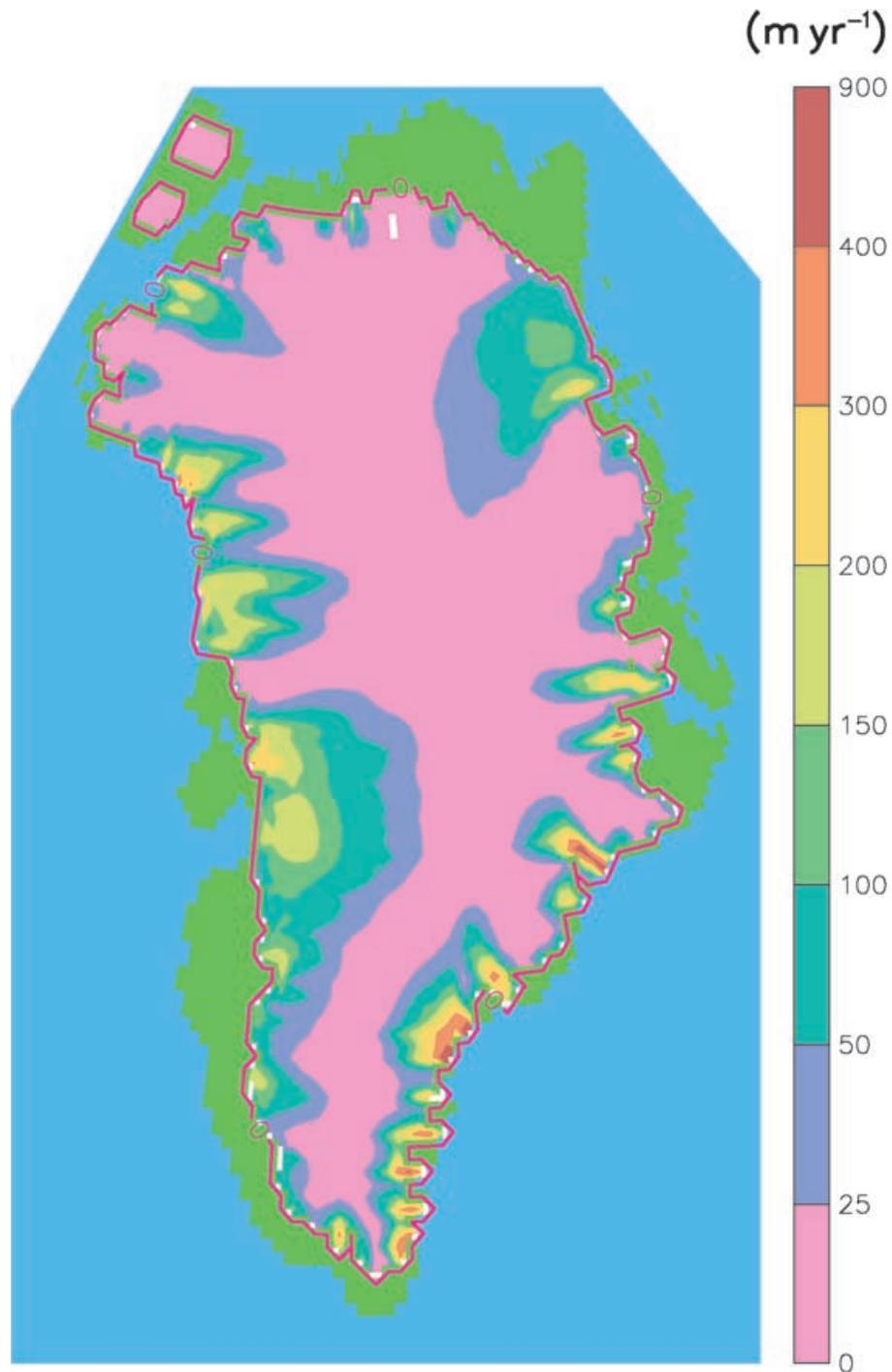
Figure 6. Computed present day ice surface velocity from model GrB.

The Sondre Stromfjord sites (05 and 06) are very close to each other, and we could not obtain a closer match to the data from site 05 than that provided by model GrB without degrading the fit to the data at site 06. To achieve as close a match as possible to the strong curvature of the RSL record that is especially evident at site 05, we enforced fast reglaciation of the region by decreasing ΔT_{adj} from 10°C to −2°C over a 1 kyr span starting at −8 kyr. This site is also in the broad region of fast flow (associated with warm basal ice, Fig. 6) stretching from north of Disko to Kapisigdlit. The physical justification for such strongly enhanced local forcing may once more be connected to the lack of fully resolved fast flows. Analyses based on ^{14}C dated moraines also suggest a highly dynamic regional ice margin with numerous Holocene
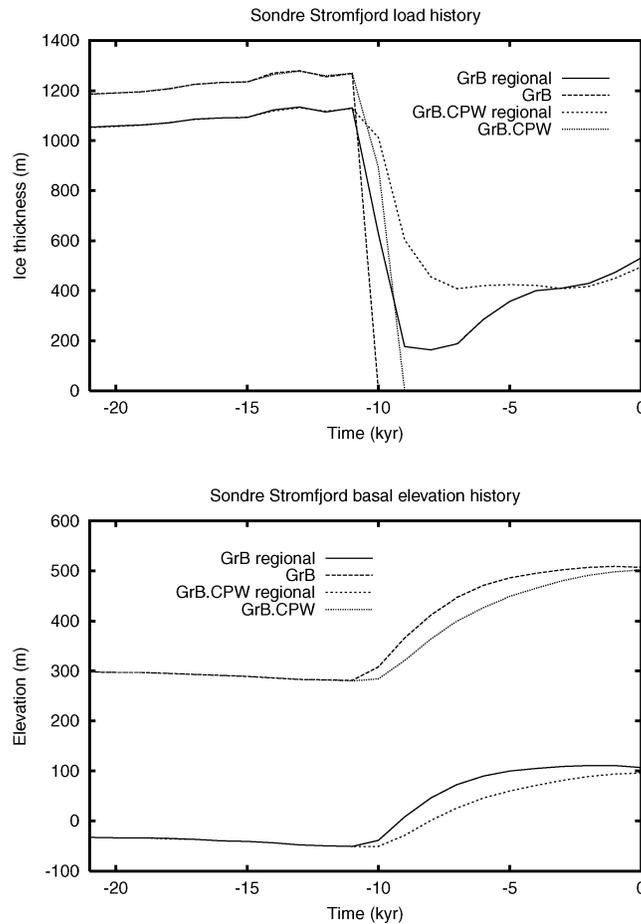
Figure 7. Sondre Stromfjord Holocene regional and grid-cell ice thickness and basal elevation chronologies for the fully tuned model GrB and for the untuned model GrB.0. Regional averages were determined using a 12° longitude by 6° latitude box.

re-advances during the last deglaciation including two significant re-advances between 4.8–4.4 kyr BP and between 2.5–2 kyr BP (Ten Brink & Weidick 1974). However, model GrB displays its strongest re-advance prior to −5 kyr with a final advance between −1.9 and −1.8 kyr. Therefore, given the excellent match to the RSL observations, the assumption of the validity of the inferred RSL envelope implies that RSL constraints are not able to clearly resolve such details of margin displacement.

To better understand the physical basis for the improvement in the RSL match at the Sondre Stromfjord sites, it is worthwhile examining the local time-series for ice thickness and basal elevation for the models with (GrB) and without (GrB.CPW) regional Holocene surface temperature tuning. Fig. 7 compares the corresponding time-series for both the gridpoint and the region. Given that the lithosphere has significant non-local influence out to a distance that is approximately four times the lithospheric thickness, our regional average time-series for ice thickness was determined over a 12° longitude by 6° latitude box. Model GrB deglaciates Sondre Stromfjord about one kyr earlier than GrB.CPW. There is also a much stronger and more extensive deglaciation of the region allowing significant reglaciation post −8 kyr. The stronger load variations result in earlier and stronger basal elevation changes and post −2 kyr subsidence of the grid-cell. These differences in basal response are directly translated into the increased concavity of the GrB RSL curve.

Kapisigdlit and Nerutussoq suffer from few data points but also suggest strong curvature in their envelopes and were therefore tuned so as to conform with neighbouring sites. The single data-point for Julianehaab has little significance. Furthermore, the proximity to Nerutussoq makes a simultaneous match of this data point and the Nerutussoq envelope unlikely. On this basis we suspect that the Julianehaab data-point may be erroneous.

The two adjacent eastern RSL sites (Mesters Vig and Skeldal) are situated almost downstream of summit. The large scatter precludes any definitive identification of the correct RSL envelope. These two sites are located just a degree north of the Scoresby Sund fjord which is the largest single eastern outlet for inland ice (Funder & Hansen 1996). Though the model likely under-represents the regional ice drainage, it does resolve an ice stream draining into Scoresby Sund (Fig. 6). The proximity of ice streams and the deep fjord of Scoresby Sund creates strong model sensitivities to the regional calving parameterization. We were only able to obtain a theoretical prediction of the RSL envelope that satisfactorily accords with all of the data points at Skeldal and most at Mesters Vig with a low value of the regional calving parameter that allowed Scoresby Sund to fully glaciate. Geological data indicates that the Scoresby Sund fjord was indeed fully glaciated at −16 kyr but it and adjacent regions were already largely free of grounded ice by −11 to −10 kyr (Funder & Hansen 1996). However earlier studies
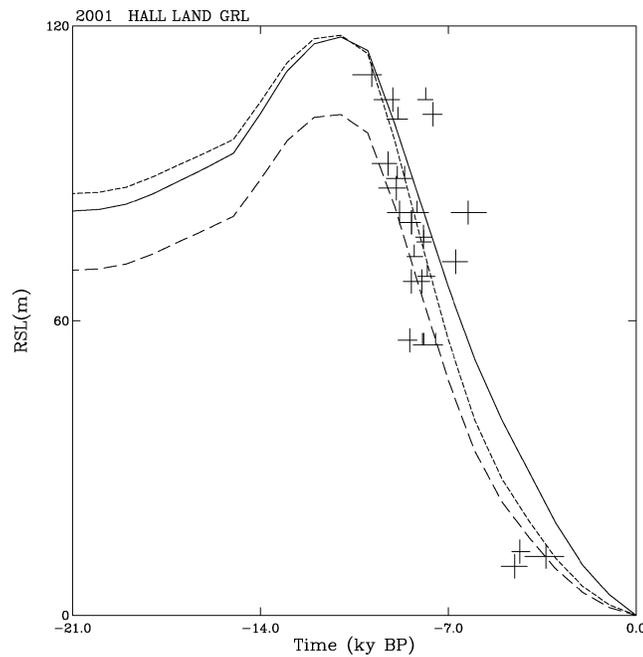
Figure 8. Hall Land RSL data-points and computed chronologies for models with increased calving strengths. Model GrBnc100 (medium-dashed line) uses a calving parameter of 100 m yr^{-1} and only allows glaciation across the centre of Nares strait. Model GrBn (short-dashed line) has a calving parameter of 0.5 m yr^{-1} that allows glaciation across the northern sector of Nares strait as well. The base GrB model RSL chronology is given by the solid line and has complete glaciation across the whole of the strait including Kane Basin to the southwest.

suggest that Mester Vig (Washburn & Stuiver 1962) and Skeldal (Lasca 1966) were not open to the sea until between −10 kyr and −9 kyr. Our model deglaciates the strait between −11 kyr and −10 kyr (Fig. 9a) in close correspondence with the chronology of Funder & Hansen (1996). The topographic details of this region result in a high degree of sensitivity to the calving parameter. Even a relatively small increase of the local calving parameter from 0.03 to 0.06 yr^{-1} produces a major reduction in the computed RSL amplitude (not shown) for these two sites. Given the data-point scatter, an RSL envelope with even stronger curvature could be chosen. However, we could not find a model tuning for a 90 km lithospheric thickness that would produce a faster response without a significant loss of RSL amplitude. Though a suitably strong curvature in the RSL record might be achievable with better representation of calving dynamics and fast ice flows, given the RSL data-point scatter, we have elected not to 'over tune' the fit to the data in this region.

The north-northeastern sector of the model was tuned only by invoking an increase in the sensitivity of precipitation to surface temperature change. In both the model (Fig. 9) and according to geological observations (Funder & Hansen 1996), the northernmost part of the ice sheet did not expand much beyond the coastline during the last glacial cycle. The proximity of especially sites 13 to 16 to each other (Fig. 4), combined with the non-local nature of bedrock displacement, places severe limits on how much the RSL response could be differentiated between these sites using physically reasonable local tuning. Thus, even with the data-point scatter and small number of data-points for the most northerly sites (15 and 16), the envelopes obtained are arguably reasonably constrained.

An offshore glacial ice cap arises in all models independent of tuning. Both GrB.0 and GrB produce a small ice cap near the seaward margin of the shelf off the northeast coast of Greenland during glacial periods, as shown in Figs 4 and 9(a). The existence of such an ice cap largely rests on the validity of the bathymetry. The input bathymetry for the model (from the ETOPO5 data set) has a shallow rise in this region with a depth of less than 25 m. As such, calving can't inhibit glaciation of this region in the model. However, there is a clear discrepancy in the shelf bathymetry between that of ETOPO5 (not shown) and that of the newer International Bathymetric Chart of the Arctic Ocean (http://www.ngdc.noaa.gov/mgg/bathymetry/arctic/arctic.htm). Therefore, it is quite possible that there is an error in the ETOPO5 data set. Furthermore, observations suggest that the shelf was unglaciated, though there currently is no way to definitely disprove the existence of such a small off coast ice cap (Funder, pers. comm.).

Geological estimates of the extent of the pre-Holocene glaciation of Nares strait have been significantly revised in the recent past. England (1976, 1985), for instance, had previously argued for a strait that was largely ice free through the last glacial cycle. On the other hand, Zreda *et al.* (1999) have recently provided evidence for the complete glaciation of the strait between −23 kyr and −10 kyr based on cosmogenic ^{36}Cl surface exposure ages of erratics and bedrock on islands in the strait. Based on a broad review of regional geological, RSL, and geomorphological data, England (1999) has fundamentally revised his own position and now also argues for complete glaciation of Nares strait including the southwestern sector (Kane Basin). In our analyses, the strongly reduced model calving in Nares strait was necessary to allow complete glaciation across the strait to Ellesmere Island to occur, as shown for the fully tuned model GrB in Fig. 9. This allowed an excellent match with the RSL data for the site adjacent to Nares strait (Hall Land). Model GrB.0, on the other hand (which has a space independent calving parameter k_C set to 0.5 m yr^{-1}) allowed glaciation only across the mid-section of Nares strait (or Nares strait proper
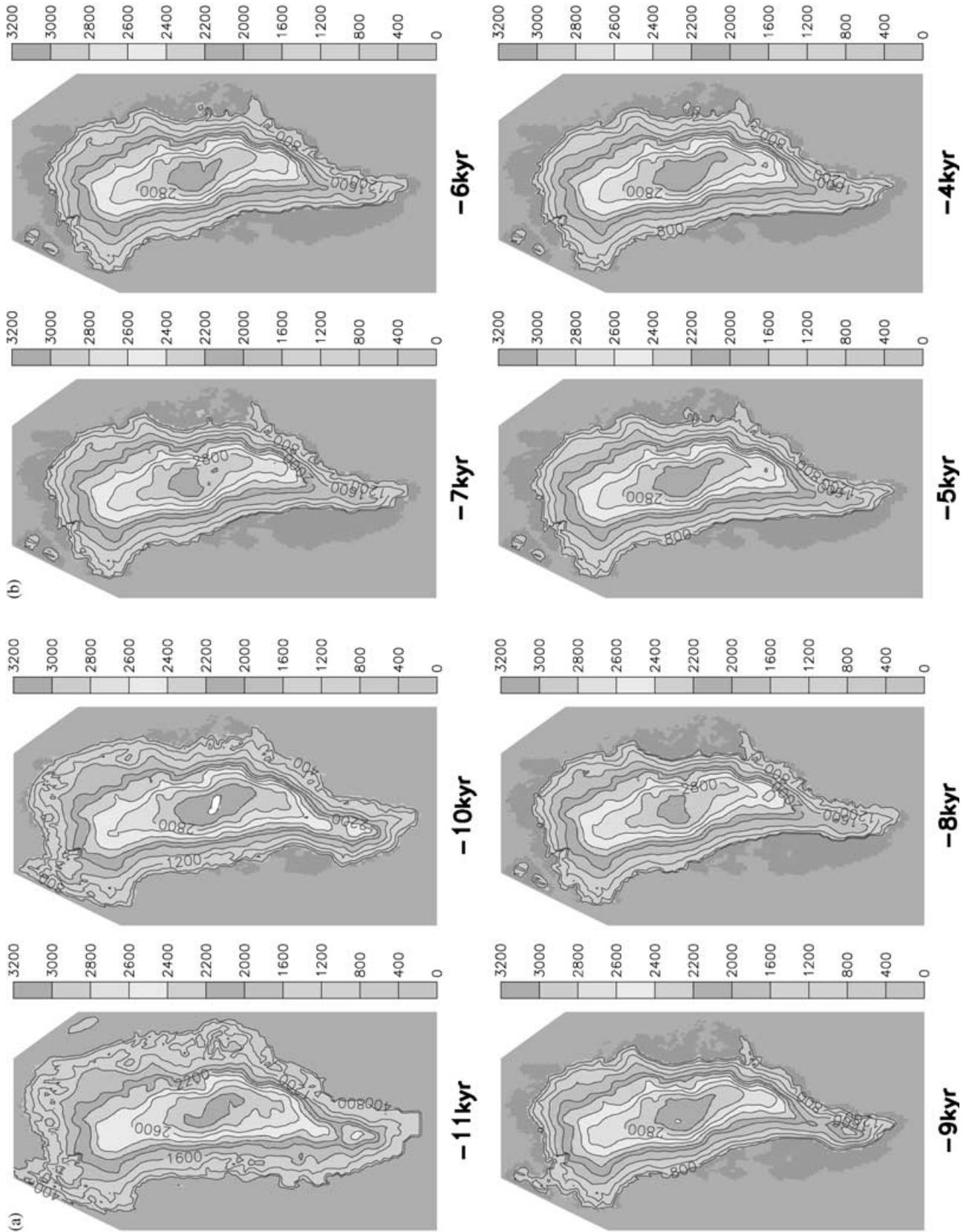
Figure 9. Model GrB ice thickness fields for early- to mid-Holocene.

according to England 1999) and had an insufficient RSL response for Hall Land. However, given the available tuning degrees of freedom, this alone provides only a weak constraint on the extent of Nares glaciation. In fact, using a value for the calving parameter of 0.5 m yr^{-1} in the fully tuned model, along with a factor of 2 regional reduction in the precipitation sensitivity (which thereby increased glacial precipitation), and a 6.0°C peak regional Holocene temperature forcing in the north-western region, does allow an excellent match to the RSL data (model GrBn illustrated by the shorted-dashed line in Fig. 8). For this case, the south-western sector of Nares strait (Kane Basin) remains ice free, however the mid to north-eastern sectors are fully glaciated. Modification of GrBn to remove north-eastern ice from the strait using an extremely large calving parameter of 100 m yr^{-1} still delivers glaciation of the central sector of Nares which is thus unavoidable in our model. For this case, the RSL response matches only the inner envelope of the data (GrBnc100, solid line in Fig. 8) and is thus likely insufficient. Subject to better constraints on the envelope, our results therefore support glaciation of at least the central and north-eastern parts of Nares strait.

The only significant remaining RSL discrepancy is that which exists for the Carey Islands. This is clearly attributable to the input boundary conditions. The islands are located just beyond the 400 m bathymetric perimeter of the input topography and thus no land surface exists in the input topography. As such, the calving model prevents ice buildup in this region. The actual islands are only about 2 km in diameter, an order of magnitude below the model resolution. Higher resolution maps (Blake 1977) indicate a greater than 500 m bathymetric trough separating the islands from the adjacent coast to the northeast which makes coastal ice expansion out to the islands unlikely. Furthermore, geological evidence also appears to preclude mainland ice expansion onto the adjacent continental shelf (Funder & Hansen 1996). However the presence of glacial erratics on island plateaus of numerous rock types that are foreign to the island geology (Blake 1977) make it clear that ice did expand out to these islands, though dating of this ice expansion remains problematic (Kelly *et al.* 1999). The presence of erratics from the Wolstenholme Fjord drainage area to the east (Kelly *et al.* 1999) indicates that grounded or shelf ice from the adjacent fjords did at some point extend to the islands. The geomorphological evidence (striations and lee side plucking) point to a general north to south ice flow over the island which would have implied glaciation over regions deeper than 200 m at LGM and/or very extensive ice shelves. This would have required a large ice flux into the region to balance calving losses. More specifically a large ice stream from Nares strait (Kane basin region) would have been required, further validating the concept of significant glaciation of Nares strait. Recent estimates (Funder, pers. comm.) place the terminal position of the grounded ice as far out as the 600 m bathymetric contour of Baffin Bay.

One noteworthy discrepancy between model and observations arises when considering independent maps of marine limits. Observations (Funder & Hansen 1996) indicate a significant increase in the marine limit (i.e. the maximum RSL) as one progresses from the present day ice margin towards the coast. However, the model displays the opposite behaviour with, for instance, Sondre Stromfjord model marine limits of 155 and 169 m respectively for the western and eastern (nearer margin) sites. This discrepancy between model and observed marine limit patterns was consistently found in the entire southwest sector of Greenland. In a simple monotonic deglaciation scenario, it would be difficult to understand the physical basis for such observations. Near-margin locations would have been exposed to more recent and stronger ice load variations and thus would be expected to display a stronger RSL signature. However, significant late Holocene re-advance would reduce the amplitude of the near margin RSL response more than that of the coastal response. Thus the observed pattern of marine limits further validates the hypothesis of significant Holocene reglaciation in the entire southwest sector. Furthermore, the lack of increase in model marine limits towards the coast strongly suggests that reglaciation occurs too early in the model. Indeed a number of observational studies (Weidick *et al.* 1990; Weidick 1993; Van Tatenhove *et al.* 1996) suggest minimal margin extent for the southwest sector at about −4 kyr as opposed to the −8 to −7 kyr period of minimal margin extent in model GrB. Aside from this discrepancy, the modelled and observed sea level marine limits are generally in agreement except for a somewhat excessive marine limit predicted for K. Christian Land (100 m for GrB as opposed to a range between 40 and 80 m according to Funder & Hansen 1996). The observed marine limit for Hall Land (about 120 m) also further invalidates the low glaciation scenario for Nares strait (model GrBnc100, discussed above) which has a marine limit of only 102 m.

The fully tuned model that we have herein derived provides an excellent match to the RSL record for all sites aside from Carey island and Julianehaab. The major improvement in the match with the observed RSL records is largely linked to changes in the post LGM pattern of margin migration for all but the northern sites (where Holocene surface temperature adjustments were generally not required). Both the fully tuned GrB model and the untuned (with respect to the RSL record) GrB.0 model have late glacial margins at or just beyond the present day coastline except for the complete glaciation of Nares strait in GrB (Figs 4 and 9). Ice volume and summit thickness (Fig. 10) then grows until the beginning of the Holocene. GrB invokes slightly earlier and much stronger deglaciation reaching a minimum ice volume and margin extent at about −8 kyr. The strong early to mid-Holocene deglaciation then allows more extensive reglaciation to occur than in GrB.0.

The significant improvement in the match with inferred RSL histories between models GrB.0 and GrB involved only relatively small changes to the large-scale characteristics of the computed present day ice-sheet. Changes in ice volume and area were less than one per cent. The reduction in net mass-balance is entirely the result of an added post −500 yr 0.29°C/century warming to the ice-sheet flanks (below 2000 m above sealevel (masl)) to obtain an intentional near-zero present day mass-balance (see later section). This additional warming had no discernible impact on computed RSL histories.

Model GrB was tuned primarily to match RSL observations and GRIP borehole temperature and age profiles which limited somewhat the achievable topographic match with the observed Greenland ice-sheet. Just the same, GrB provides a reasonable match with an area-averaged root-mean-square (rms) error of only 79 m compared to the topographic data set of Bamber *et al.* (2001) (entry σ_K in Table 4). The more significant regional discrepancies with respect to the observed ice-thickness field are characterized by excessive margin thickness to the north-northwest and east, and slight insufficiency in margin extent in the south-southwest and northwestern and northeastern tips (Fig. 3). Ice area is thereby underestimated by about 2 per cent (Table 4). The overestimation of present day ice volume by GrB (3.08×10^{15} m^3) is similar to that obtained in other current modelling studies (e.g. Huybrechts & de Wolde 1999).
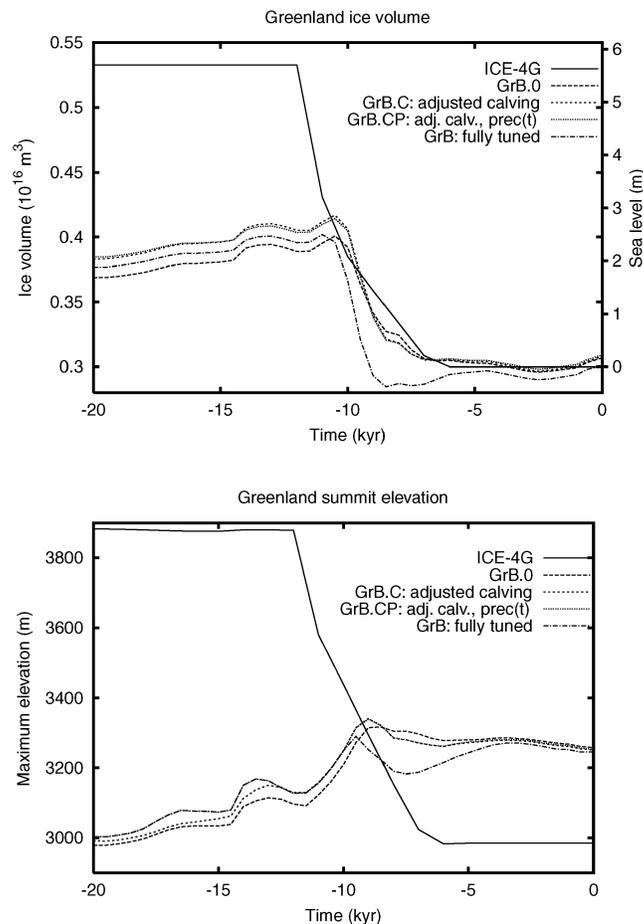
Figure 10. Computed ice volume and sea level equivalent chronologies for ICE-4G and GrB models.

In order to further illustrate the model sensitivity to the regional temperature adjustment ΔT_{adj}, we provide computed RSL histories for two more sensitivity runs. Model GrB.6Tm assumes a value that is 60 per cent of that assumed in GrB and model GrB.1 kyl imposes a 1 kyr lag on ΔT_{adj}(GrB, t). The results for both GrB.6Tm and GrB.1 kyl are shown in Fig. 11 (the medium and short-dashed curves respectively). The imposition of a 1 kyr lag on ΔT_{adj} generally results in a small increase in the RSL maximum and a concomitant effective lag in the RSL decrease resulting in poorer fits for all regions covered by ΔT_{adj} aside from Hall Land (no impact) and Disko where data-point scatter makes definitive inference of the RSL history impossible. The 40 per cent reduction of ΔT_{adj} has a smaller impact except for a significant reduction in the RSL amplitude for Nerutussoq Cw and slower RSL decrease for Sondre Stromfjord and for the eastern sites (Mesters Vig and Skeldal). The tuning to obtain the high quality RSL fit that is delivered by GrB is of course by no means unique. However these results do show that the strength of ΔT_{adj} forcing cannot easily be downgraded without some associated reduction in the quality of the fit to the RSL data.

One other issue raised by the model results is the question of the uncertainties arising from the simplified calving model and the relation of this to the area extent of the LGM model ice sheet. Model GrB has an LGM extent of grounded ice of 2.43×10^{12} m^2. With reduced regional calving in certain regions, we can obtain LGM model extents of 2.54×10^{12} m^2, with only a slightly weaker fit to the RSL data (not shown). Other recent models using different calving parameterizations tend to have larger areal extents between 2.6 and 2.7×10^{12} m^2 (e.g. Cuffey & Marshall 2000; Huybrechts 2002), while a compilation based on observational evidence estimates LGM areal extent at roughly 2.76×10^{12} m^2 (Funder, pers. comm.). The issue involves the discrepancy in the extent of ice expansion onto the continental shelf, a region where data is limited. Furthermore, asynchronous surge events could result in evidence for extremal margin extent that would suggest a larger grounded ice area than actually existed at any one time. By reducing the maximum strength of the calving parameter in the model (k_C) to 0.03 m yr^{-1} per m of buoyancy, we can obtain an areal extent of 2.63×10^{12} m^2. However, the large expansion of ice onto the continental shelves off the southwest and northeast coasts of Greenland results in excessive RSL response for the Disko, Sondre Stromfjord and K. Christian Land model sites, even with Holocene temperature forcing adjustments removed. Disko Island and Disko Bugt, for instance, have computed marine limits of 165 and 201 m respectively with this reduced calving model. The significant extension of grounded ice off the northeast coast in the reduced calving model is also not supported by observations which indicate that glaciation was restricted to outlet glaciers with adjacent uplands free of ice cover (Funder *et al.* 1998). The key point here is that RSL constraints leave little room for LGM ice-expansion in the southwest and northeast beyond that of model GrB. However, as discussed above, data from the Carey Islands indicate that the region to the south of Nares strait had significantly more ice expansion then is possible in the model. More ice expansion off the southeast coast may also
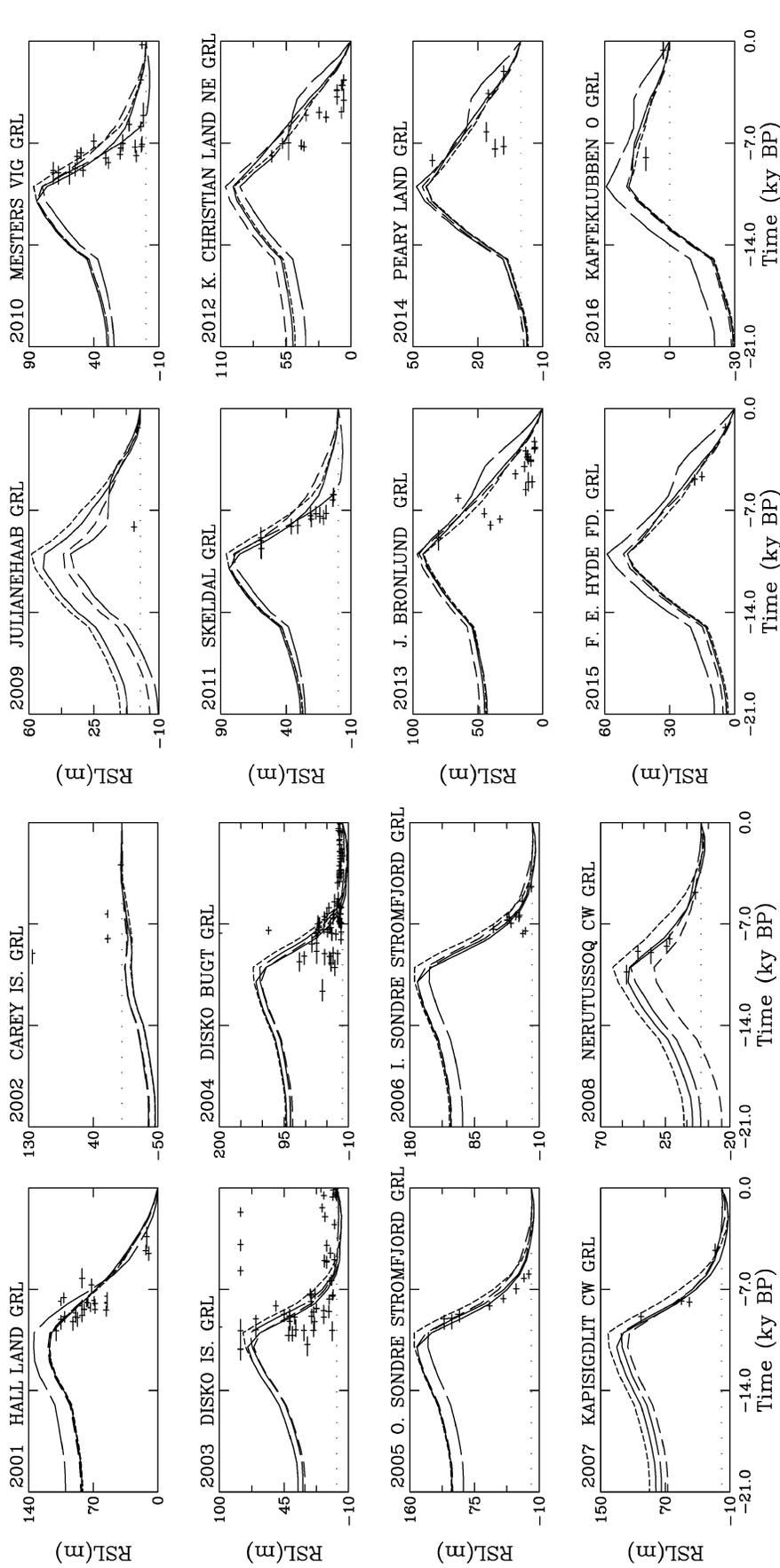
Figure 11. RSL data-points and computed chronologies for models Gr35L12 (retuned for fit with 120 km lithospheric thickness, long-dashed line), GrB.6Tm (GrB but with Holocene temperature adjustment T_{adj} reduced by 40 per cent, medium-dashed line), GrB.1kyl (GrB but with a 1 kyr lag on T_{adj}, short-dashed line), and GrB (fully tuned base model, solid line).

be valid (Funder *et al.* 1998), however the absence of RSL data for this region limits the constraint possible within the context of the present modelling analyses.

4.2 Comparison with ICE-4G

The constraints on the history of the Greenland ice sheet provided by the RSL data as illustrated above are most relevant to the loading and unloading history near the ice-sheet margin. This is especially evident if we compare the GrB model 0–16 kyr ice thickness anomaly field (i.e. H(−16 kyr)–H(0 kyr)) with that of the ICE-4G model. The ICE-4G model delivered similar or even weaker RSL responses (Fig. 13) in the west to southwest compared to that of model GrB, however ICE-4G imposes 400 to 800 m of extra ice load change over the southern core of the ice mass (Fig. 12). Model GrB has its strongest ice load changes beyond the present day margins of the ice-sheet. ICE-4G on the other hand imposes a large-scale decrease in ice thickness at −16 kyr (relative to present day) over the whole core of the ice-sheet in contradistinction to GrB (and other dynamic ice-sheet models) that has a thickening of the core largely due to an increase of precipitation with warmer air temperature.

These differences in load distributions carry over to the total amount of load change simulated. All the dynamic models deglaciate about half as much ice as the ICE-4G reconstruction (Fig. 10). Aside from the amplitude, the chronology of Holocene ice volume change for ICE-4G is similar to all models except GrB for which significant reglaciation occurs beginning at approximately −7 kyr. The earlier (effectively pre-Holocene) start of the ICE-4G deglaciation is likely due in part to the older ^{14}C calibration used for that model's tuning target.

Overall, the ICE-4G and GrB ice load differences are most significant for the core region of the ice sheet, where the ICE-4G reconstruction was unconstrained. The variations of the load in ICE-4G from −16 kyr to present are largely within 400 m of those of the GrB model in regions external to the present day margins that have nearby RSL history constraints. These results further emphasize the local nature of RSL constraints for present day ice-sheets. It should be noted that this is not the case for near-core RSL observations (e.g. Laurentide, Fennoscandia and the Barents Sea) where constraints on regional load histories would have a definite large-scale impact on the ice sheet reconstruction and for which, therefore, the geophysical inversion of RSL data delivers strong constraints on macroscopic ice-sheet form.
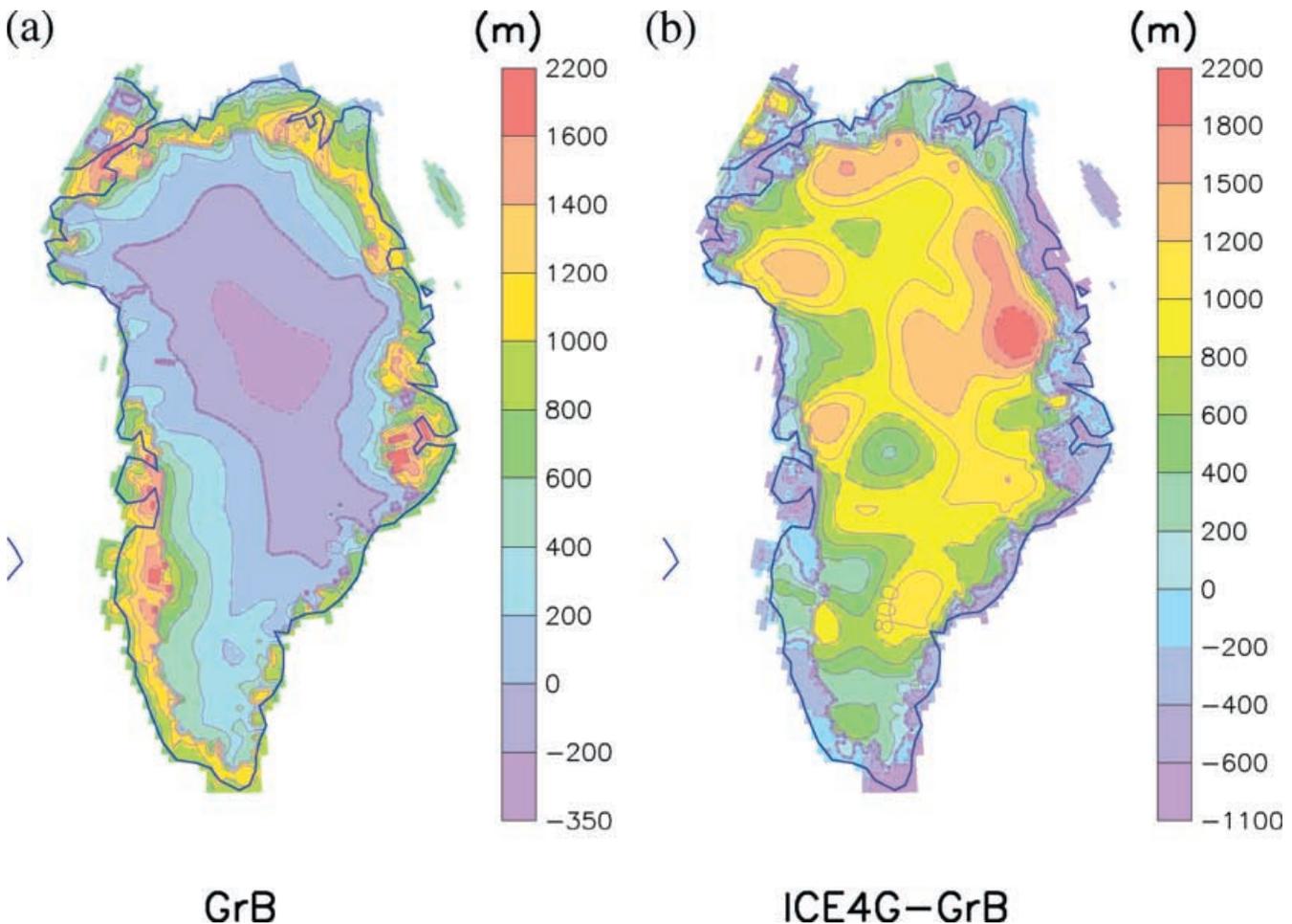

Figure 12. Comparison of GrB modelled ice load change with ICE-4G: (a) 16 kyr BP ice thickness excess relative to present (i.e. H(16 kyr BP)–H(present)) for model GrB and (b) ice thickness excess difference between model ICE-4G and GrB.
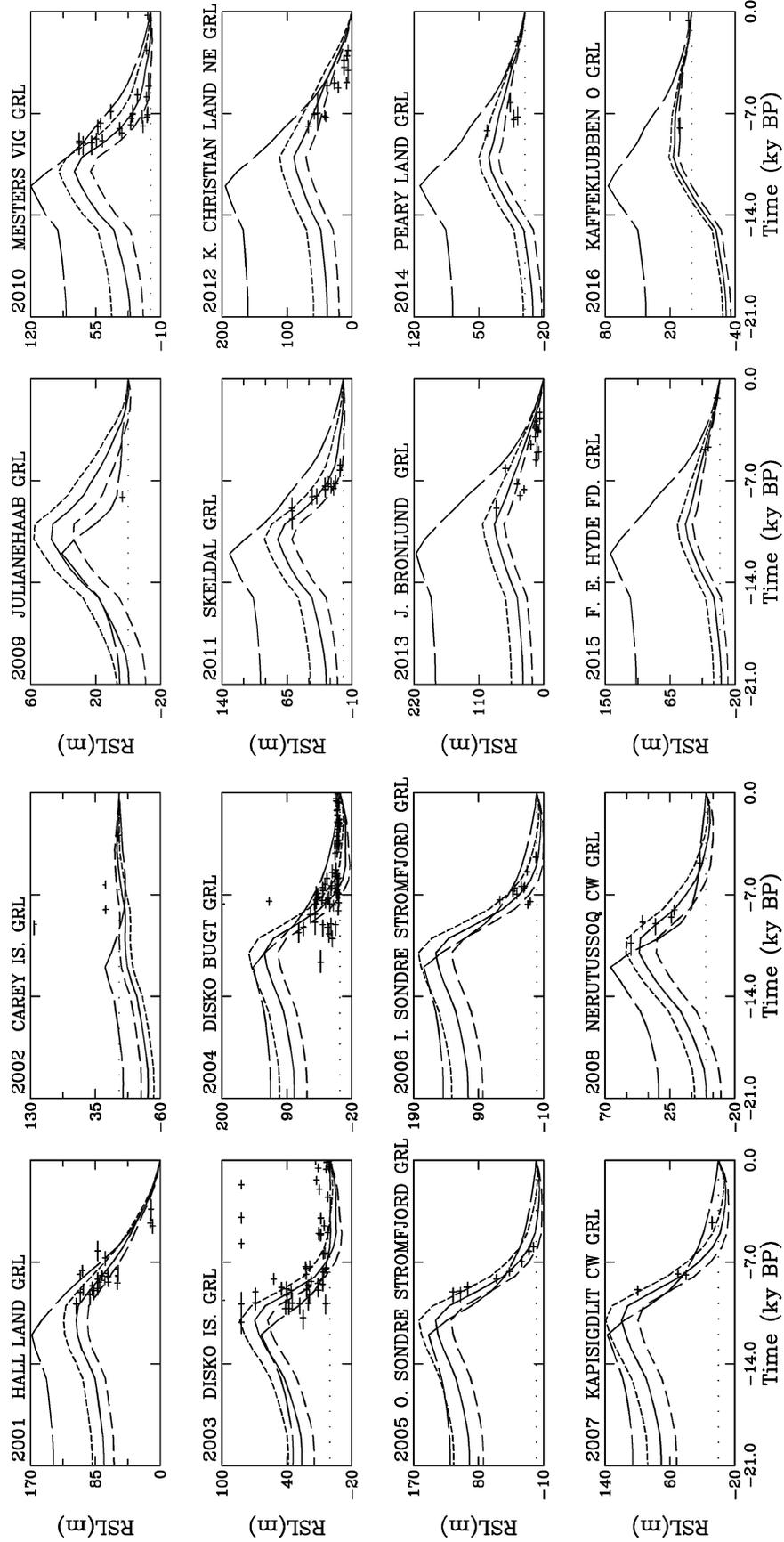
Figure 13. RSL data-points and computed chronologies for ICE-4G (long-dashed) and GrB models with respective lithospheric thickness of 120 km (medium dashed), 100 km (solid line) and 80 km (short dashed).

4.3 Sensitivity to lithospheric thickness

The computed ice-sheet history has been found to have relatively low sensitivity to the lithospheric thickness used in describing the isostatic adjustment process in the model. Present day ice volumes for model runs with lithospheric thickness ranging from 80 to 120 km were respectively 3.06×10^{15} m^3 and 3.11×10^{15} m^3, i.e. less than a 2 per cent difference. However the impact on computed RSL histories was found to be significant. The RSL response is of course found to be strongest for models with a thinner lithosphere (Fig. 13). Only the most northerly site (Kaffeklubben) is insensitive to lithospheric thickness. For all of the remaining sites, the model with a 120 km lithosphere generally delivers an overly weak RSL response (aside from the poorly constrained one to two data-point sites of Julianehaab and F.E. Hyde). Given that the GrB model was tuned for a 90 km lithosphere, this demonstration does not of itself rule out the possibility of a thicker lithosphere.

In fact, with a stronger Holocene climate forcing (T_h for Disko, Sondre, Kapisigdlit, Nerutussoq, and east increased to 13, 13, 12, 15, 15 and 8°C respectively and a 12°C regional ΔT_{adj} for the north-northwest (around Hall Land) together with a reduction of the precipitation sensitivity to surface temperature to 0.6 times the default value of η for the whole northern sector (north of 79°N, a close match to the RSL curves of GrB and thus to the observations) is obtainable with a 120 km lithosphere with arguably an even better match to data from the eastern sites (Mesters Vig and Skeldal) depending on which envelope is inferred from the data (Model Gr35L12 in Fig. 11). Only the northeastern sites have a poorer match, which could be remedied by better tuning (i.e. by increasing the precipitation sensitivity to surface temperature change). The stronger eastern and western temperature forcing result in more core ice depletion and, to compensate, the flow enhancement parameter was reduced to 4.8. The final volume of 2.99×10^{15} m^3 is also closer to the observed value. The mid-Holocene low to present ice volume difference has now increased to 2.41×10^{14} m^3 or about 0.6 m of eustatic equivalent. To assess the plausibility of this thick lithosphere solution as compared to the thin lithosphere solution embodied in GrB we need to assess the plausibility of the increased strength of the temperature forcing. Values of ΔT_{adj} of 15°C (as required for the Gr35L12 model) are arguably difficult to accept. However, given that these temperature forcing modifications are in part compensating for the lack of explicit ice stream/outlet glacier mechanics, such forcings cannot be entirely ruled out. A more definitive test of the physical acceptability of the tuning must await more detailed analyses employing models with explicit ice stream mechanics.

Aside from possibly Kapisigdlit, the model with the thin 80 km lithosphere (short dashed line in Fig. 13) provides generally no better or even a slightly poorer fit to the RSL observations than that of the base GrB model with a 90 km lithospheric thickness (solid line in Fig. 5). However, again it must be remembered that the model was tuned for a 90 km thick lithosphere and slight tuning modifications would almost certainly allow the model with a 80 km thick lithosphere to deliver the same or better quality fit. It is generally easier to tune models with thinner lithospheric thickness to the RSL record given the more local bedrock response that ensues. As such, it is much more difficult to rule out thinner lithospheric thicknesses with the methodology employed.

As a test of the sensitivity of the results to the bedrock model employed, GrB was rerun with a local damped relaxation type bedrock model with time constant 4.5 kyr as employed in Tarasov & Peltier (1999). This (GrBb in Table 4) resulted in only a 2 per cent reduction in computed present day ice volume to a value closer to that observed and similar maximum elevation. This lack of significant sensitivity of ice-sheet evolution to the type of bedrock representation employed is in keeping with the low ice sheet sensitivity to the thickness of the lithosphere in the global viscoelastic bedrock model. These results also agree with previous analyses for Laurentide and Eurasia (Tarasov & Peltier 1997b) that also suggested much reduced sensitivity. The significant 9 m reduction in rms difference between observed and model topography (σ) is likely at least partly due to the higher effective resolution of the local bedrock model.

5 GEODETIC TESTS OF THE VALIDITY OF THE NEW GLACIAL HISTORY FOR GREENLAND

Since the issue of the quality of the new reconstruction of the late-Pleistocene glacial history of Greenland can only be tested by investigating its ability to explain observations not employed to construct it, we investigate this issue herein by examining whether or not recently obtained geodetic constraints are in accord with model predictions. There are two primary types of such constraints which are available to us, respectively GPS observations of the present day rate of radial displacement of the solid Earth, and present day regional mass-balance in the accumulation zone computed using observed precipitation and GPS-derived 2000 m elevation mass-fluxes. We will discuss the ability of our new model of Greenland glaciation history to reconcile each of these types of observation in turn.

5.1 GPS measurements and model-derived present day rates of radial displacement

RSL histories are a signature of the competition between three distinct processes: bedrock displacement, geoid adjustment, and ocean volume change. Recent advances in Global Positioning System (GPS) measurements now allow direct measurements of bedrock displacement rates, both vertical and horizontal. Long-term GPS measurements from 3 coastal sites on Greenland (Wahr *et al.* 2001, 2002) may be invoked to provide an independent check and/or tuning target for the deglaciation model.

The predicted present day rate of vertical displacement delivered by model GrB is characterized by widespread subsidence over all but the northern and north western sectors and mid-eastern tip of Greenland (Fig. 14) with an ice-sheet average displacement rate of 1.0 mm yr^{-1} downward. Also shown on this Figure is the background bedrock response due to the non-Greenland components of the ICE-4G model and the 'correction term' that has been added to the basal displacement rate computed by the coupled ice-sheet and bedrock model. This correction
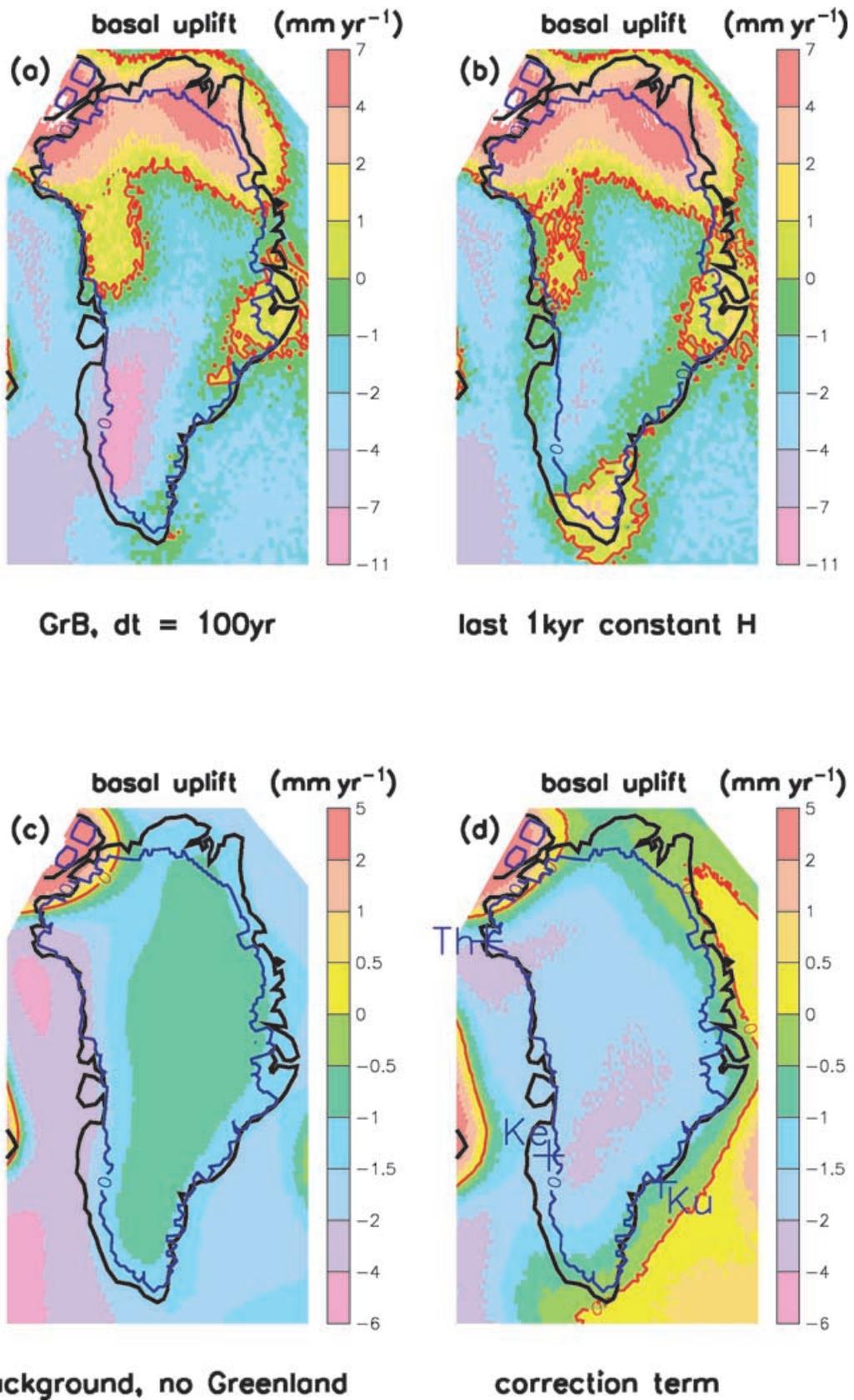
Figure 14. Rate of basal uplift over last 100 yr for (a) model GrB and (b) for model GrB but with ice field frozen for last 1000 yr. Also shown are (c) the contribution to the rate of present day basal uplift from the non-Greenland components of ICE-4G and (d) the correction term for computing full rate of basal uplift that includes both ICE-4G non-Greenland and non-eustatic ocean load components (refer to text for details).

Table 5. Present day basal uplift for coastal stations (mm yr^{-1}) for various models and from observations. Included are range limits and averages from a suite of 10 slightly different models with similar RSL chronologies as described in the text. Model GrB.r has the identical parameter configuration as the base model GrB but was initiated with less thermomechanical equilibrium at −250 kyr. Model GrB.Th0 also has identical parameters as GrB except that no constant regional Holocene cooling is imposed in the vicinity of Thule. Model GrB.E66 uses a weaker δ^{18}O to climate inversion ($\alpha_c = 0.66$) during the Eemian to increase minimum Eemian ice volume. Model GrB.H1 k imposes constant ice load during the last 1kyr and GrB.CPW does not incorporate the ΔT_{adj} forcing. The GrBw series of models have altered late Holocene imposed extra warming. Model GrBw3b imposes only a 0.3°C warming over the last 100 yr (instead of 0.29°C/100 yr over the last 500 yr). Model GrBw0 has no extra post −500 yr warming and model GrBwk0 has, in addition, not post −1.2 kyr extra warming. Refer to text for details.

Model	Kellyville	Kulusk	Thule	Ice-sheet average
Observed[a]	−5.8 ± 1.0	−2.1 ± 1.5	−0.7 ± 0.9	
GrB.direct	−3.8	−0.2	2.0	0.6
GrB	−5.6	−1.0	0.1	−1.0
GrBw3b	−6.6	−1.8	−0.9	−1.9
GrBw0	−6.6	−1.8	−0.9	−2.0
GrBwk0	−7.2	−1.8	−0.3	−1.8
GrB.r	−5.6	−1.6	0.7	−1.0
GrB.Th0	−5.8	−1.0	−0.3	−1.0
GrB.E66	−5.8	−1.0	0.3	−1.2
10 model avg	−5.5	−1.2	0.3	−1.0
10 model low	−5.8	−1.7	−0.3	−1.0
10 model high	−4.8	−1.0	0.7	−1.2
GrB.H1k	−1.6	−0.1	0.1	0.0
GrB.CPW	0.2	−1.7	−0.9	−0.1

[a](Wahr *et al.* 2001, 2002).

term is the present-day difference in the rates of computed basal uplift between a full gravitational-self-consistent offline computation (i.e. that takes into account all contributions, including non-eustatic and non-Greenland ICE-4G load changes), and that computed by the coupled viscoelastic model (that only takes into account the viscoelastic response to ice and eustatic load variations) for a model run in which the last 2 kyr of ice load were held constant. The off-line model is only set up to run on 1 kyr increments and therefore it is inappropriate for computing present-day basal displacement rates for a model with continuously changing ice. In comparison with the available GPS observations, station displacement rates for GrB are within error bar limits for all three stations (Kellyville, Kulusk, and Thule, respectively 'Ke', 'Ku', and 'Th' in Fig. 14) (Table 5).

Present day uplift rates were found to have an order (0.5 mm yr^{-1}) sensitivity to the degree of equilibrium for the −250 kyr run initiation. For instance model GrB.r (Table 5) has an identical parameter configuration to GrB but was initiated with less thermomechanical equilibrium at −250 kyr and as a result, the basal uplift rates at Kulusk and Thule change from −1.0 and 0.1 mm yr^{-1} to −1.6 and 0.7 mm yr^{-1}. In order to give some approximate error bars and to display bedrock model sensitivities, Table 5 also shows the maximum range and average basal uplift rates from a suite of 10 different models with almost identical RSL chronologies but with differing amounts of initial thermomechanical equilibrium, slight (order 10 per cent differences in ΔT_{adj}, as well as a model with increased Eemian ice volume due to a less sensitive Eemian climate sensitivity parameter (model GrB.E66 with $\alpha_c = 0.66$ in eq. (13) above for the Eemian period). The model ranges are within observational uncertainty for Kellyville and Kulusk though the magnitude of the suite averages lie below the observed averages. The suite average for Thule, however, is just outside of the observational error bars. The modelled slight uplift for Thule is due to the constant Holocene cooling that was imposed in the region around Thule to improve margin extent there. For the model without this adhoc regional cooling (GrB.Th0 in Table 5) weak subsidence (0.3 mm yr^{-1} downward) is predicted for Thule. It would also be quite easy to tune the model for stronger regional subsidence by imposing early- to mid-Holocene warming and then subsequent cooling. But we have not imposed the GPS observations as constraints and it should therefore come as no surprise that the closest match to observations is for the Kellyville site, the only region were RSL constraints were available for the model.

Aside from model GrB.E66, all members of the suite have identical (to 2 significant digits) ice-sheet average rates of basal uplift. It should also be kept in mind from the previous discussion concerning the observed increase in marine limits as one progresses from the ice margin to the coast in the southwest sector that model GrB is likely reglaciating this region too early in the Holocene. A more recent reglaciation would increase the present day rate of basal sinking in the southwest sector of the model (where Kellyville is located).

The pattern of basal sinking predicted by our GrB model is quite distinct, however, from that of the model by Le Meur & Huybrechts (1996) which has present-day basal uplift under most of the ice sheet. This latter study involved no tuning of the glacial history so as to fit local RSL histories and incorporated only the direct load changes due to variations of the Greenland ice sheet and adjacent ocean. Because Baffin Island to the immediate west of Greenland was heavily glaciated at LGM, in the absence of the unloading of Greenland itself, this region would be controlled by the collapse of the glacial 'forebulge' outboard of Baffin Island (Fig. 14c).

The entry listed as GrBdir in Table 5 shows the direct bedrock response from the coupled model which includes the global eustatic and northern Ellesmere ice load changes but not the load changes due to the non-Greenland components of ICE-4G nor those due to changes in the

geoid. The O (2 mm yr^{-1}) site discrepancies compared to the full computation are small enough to validate the use of the simplified isostasy model for the ice dynamics but significant enough to justify the full gravitationally self-consistent computation for detailed GPS comparisons.

The exact bedrock response is of course quite sensitive to the century scale climatic forcing of the recent past. To separate the long term viscous component from the short term viscoelastic responses, Fig. 14(b) shows the 100 yr present day bedrock response for a coupled simulation with a constant ice field for the last 1000 yr. The only significant change is much reduced sinking in the southwest (the Kellyville site basal sinking rate is reduced from 5.6 to 1.6 mm yr^{-1}, Table 5) and the appearance of basal uplift in the southern tip. There is a corresponding reduction in the ice-sheet average bedrock displacement rate to 0.0 mm yr^{-1}. The modelled present day bedrock response is thus dominated by a viscous response to the long-term glacial loading history in the northern and eastern regions but has significant submillenial contributions in the southwest.

As has already been stated, model GrB has two extra late-Holocene climate forcing modifications and it is worth considering their impact on the computed rate of basal displacement. Model GrBw3b has reduced the 0.29°C/100 yr post −500 yr warming to only post −100 yr (still at 0.29°C/100 yr). Model GrBw0 has eliminated this warming all-together, and model GrBwk0 has also eliminated the post −1.2 kyr cooling and warming used to improve the model match to the top part of the observed GRIP borehole temperature profile. GrBw3b and GrBw0 both have about a 1.0 mm yr^{-1} increase in the rate of basal sinking for the 3 sites as well as for the ice-sheet average, now at 1.9 and 2.0 mm yr^{-1} (downward) respectively (Table 5). Model GrBwk0 has even a stronger response at the Kellyville site of 7.2 mm yr^{-1} downward, which is beyond the observational range. For all three GrBw models, Kulusk and Thule sites both have much closer agreement to observational mean values. The increased downward response for these three models follows physically from the short-term components of the viscoelastic response and the instantaneous elastic response to increased recent ice loading. The general agreement with observations of basal rates of displacement that is maintained or even improved (with the afore mentioned exception of GrBwk0 at Kellyville) with the removal of the more weakly constrained late-Holocene temperature forcing modifications adds further confidence in the general validity of the model. Furthermore, the increased rate of ice-sheet average basal displacement with the GrBw models suggests that the value for model GrB of −1.0 mm yr^{-1} is arguably an upper bound to the actual value.

The major southwestern subsidence of the GrB models is a result of the strong early Holocene deglaciation and subsequent reglaciation required to match the local RSL record. For the model run with no adjustment to regional temperature forcing (GrB.CPW), the computed present day basal displacement rate at Kellyville is slightly upward (0.2 mm yr^{-1}), though the ice-sheet average displacement experiences less reduction and is still slightly downward. Without the regional forcing, there is much less early- to mid-Holocene retreat of the margin and little subsequent late Holocene re-advance of the adjacent ice-sheet sector. The RSL data at the adjacent sites (Sondre Stromfjord, sites 05 and 06) also fit much more poorly with GrB.CPW. Both the GPS and RSL records therefore appear to require significant mid- to late-Holocene re-advance in this region in agreement with the hypothesis of Wahr *et al.* (2001).

5.2 Regional mass-balance

The present day mass-balance of Greenland is a topic of considerable interest given concerns about the impact of global warming on sea level rise. Two different observational approaches have been applied to Greenland. Investigations comparing the inferred ice discharge and accumulation for the region of the Greenland ice-sheet above the 2000 m elevation contour (Thomas *et al.* 2000) find near equilibrium mass-balance for that region. On the other hand, mass-balance determinations for the whole ice sheet using aircraft–laser altimeter surveys and PDD-based ablation estimates in the near-margin regions for 1993, 1994 and 1999 (Krabill *et al.* 2000) suggest a net mass loss of about 51 km^3 of ice per year. However, these latter results are dependent upon the assumed values for basal uplift under the ice-sheet, for which direct observations are lacking. The 4 to 5 mm yr^{-1} uplift rates assumed in the work of Krabill *et al.* (2000) are in clear disagreement with the results for our tuned model GrB which matches both the Holocene RSL records as well as the GPS observations presented above.

In contrast to the results of Krabill *et al.* (2000), both energy-balance analyses (e.g. Oerlemans 1991) as well as studies based on 3-D thermomechanically coupled models using PDD mass-balance schemes (e.g. Huybrechts & de Wolde 1999) generally find positive (though relatively small) present day net mass-balance. The lack of significance of the disagreement between observational analyses and model predictions is further illuminated when consideration is given to temporal variability. Analyses of 1978–1988 Seasat and Geosat satellite altimeter measurements for the southern half of Greenland (south of 72°N) find interannual variations of ±8 cm yr^{-1} in ice-surface elevation (Davis *et al.* 1998). Applying even half this value to the whole ice-sheet gives ice-volume variations of approximately ±70 km^3 yr^{-1}. Since model analyses generally use climate fields based on pre-1990 values, it is quite conceivable that interdecadal variability and current global warming could easily account for order 50 to 100 km^3 discrepancies in modern Greenland ice-sheet mass-balance estimates.

Given the simplicity of the climate forcing and mass-balance representation, the high mass-balance sensitivity to surface topography and climate forcing and the observed interannual variability, a comparison of mass-balance in lower elevation regions where ablation is active is poorly constrained. However, the mass balance in the upper elevation regions is controlled by longer timescale ice dynamics and is thus a more appropriate test region for intercomparison of glacial cycle ISM predictions and observations. We will therefore focus our mass-balance comparisons on higher elevation regions.

Without purposeful mass-balance tuning, the GrB.∗ series of models generally predict a 43 to 64 km^3 positive mass-balance for the entire ice-sheet over the last 100 yr (to 1990). Model GrB without mass-balance tuning (GrBw0 in Fig. 15a, with the 2000 masl contour indicated in red) has some significant misfits in high-elevation regional mass-balance in comparison with the results of the observational studies of
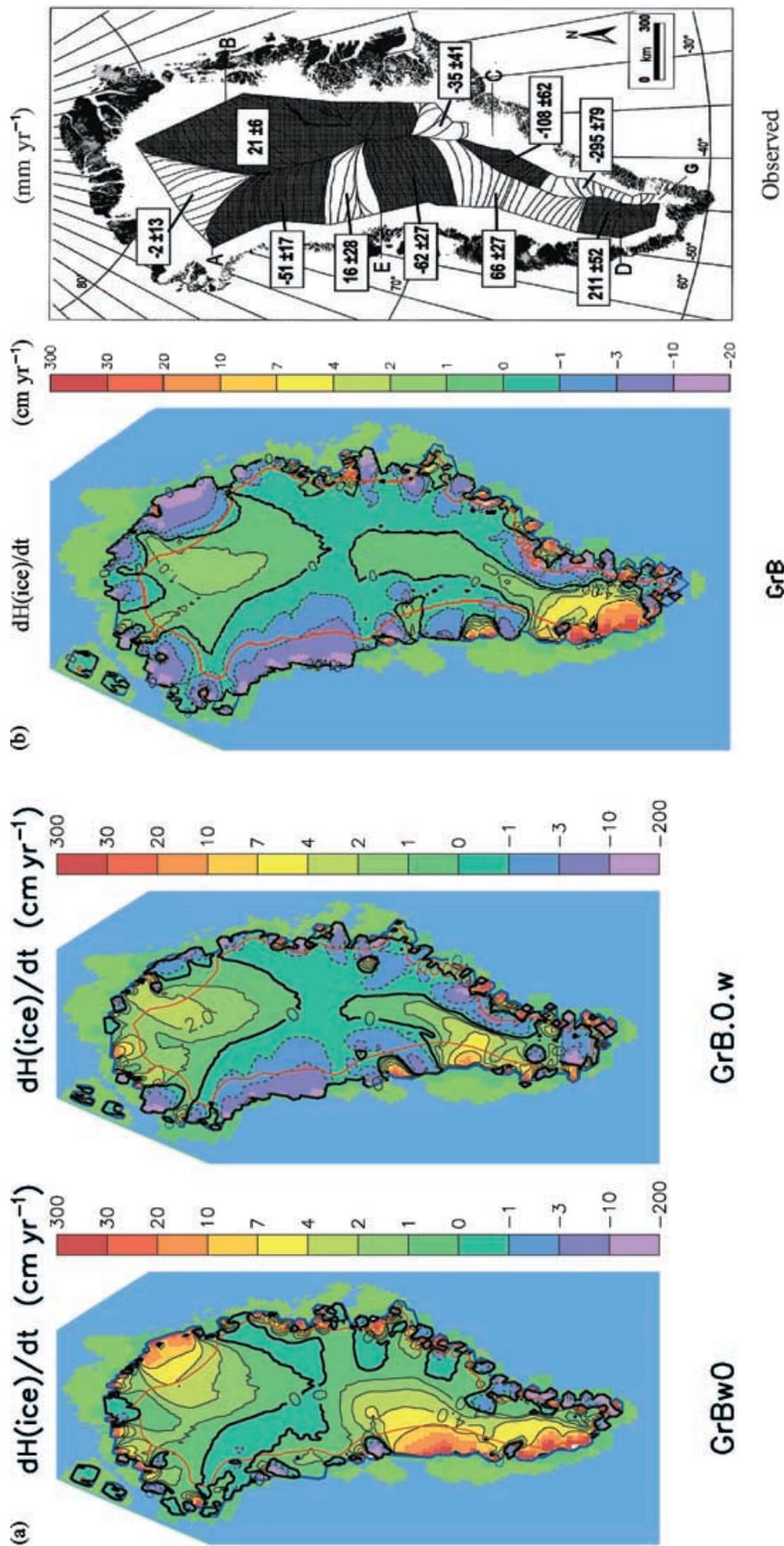
Figure 15. (a) Rate of ice thickness change over the last 100 yr from model GrB with no post-500 yr computed mass-balance. The 2000 m elevation contour is shown in red. (b) Rate of ice thickness change over the last 100 yr from model GrB with the 2000 m elevation contour shown in red. And for comparison, the observed rate of ice thickness change for the above 2000 masl region from Thomas *et al.* (2000).

Thomas *et al.* (2000), based on inferred ice discharge and accumulation for ice-sheet surfaces above 2000 masl (Fig. 15b). Most significant are the near complete lack of mass-loss along the southeastern flank (above 2000 masl) and absent or too weak mass-loss regions for central and north-central (i.e. north of 69°) west Greenland. On the other hand, GrBw0 matches within observational uncertainties the whole southwest sector (i.e. south of 69°) and the northeast sector. The model results are based on computed ice-thickness variations over the last 100 yr. In contrast, the ice-discharge component of the observational studies is based on data from a 5 yr GPS campaign (1993–1997). Given that it is only high elevation regions which are being compared, uncertainties in the comparison due to differing time periods should generally be limited.

Model GrB has been tuned to near-zero present-day net mass-balance through the imposition of a 0.29°C/100 yr warming to the flanks of the ice sheet over the last 500 yr (linearly ramped up from 0 to 1000 masl and then ramped down to 0 at 2000 masl). This results in generally good agreement with the observed mass-balance field as shown in Fig. 15(b). Such an imposed warming in a region where the climate history is poorly constrained is within the uncertainty of the climate forcing. The only significant disagreement is in the broader region of ice thinning for the eastern sector in GrB and the insufficient extent of thickening in the southwest (which is captured by GrB.0w). It should be emphasized that GrB was tuned for near 0 net mass-balance but no regional tuning to the pattern of Thomas *et al.* (2000) was imposed. Regions of current basal uplift are all associated with present-day ice thinning, however the converse is not as consistent. The southwestern flank of the ice sheet for instance has zones of both thinning and thickening, even though the whole region is experiencing major basal subsidence. This attests to the different temporal scale sensitivities of ice and bedrock dynamics.

The ice-thickness change field for the untuned (with respect to RSLs) GrB.0.w model, modified to have near-zero present-day mass-balance, displays (Fig. 15a) a similar pattern of regional mass-balance except for the complete absence of a strong thickening zone in the south-southwest and stronger thickening in the southwest. The strong south-southwestern thickening in GrB is due to the regional modification to the Holocene temperature forcing that forced strong regional mid-Holocene deglaciation and then subsequent re-advance. The associated present day basal sinking in the region then allows increased mass accumulation. However, this same argument appears to breakdown in the Sondre Stromfjord region. Here GrB.0.w has stronger thickening. This illustrates the complexities of the ice-sheet model response to model forcings.

The primary tuning target for GrB was the RSL record. Relatively small improvements were also made to the topographic match and these were largely a side-effect. But ice flow patterns (which together with precipitation control high-elevation evolution) were not a tuning target. Furthermore, the 0.29°C/100 yr warming added to tune for near-zero present-day net mass-balance was geography independent. As such, the general agreement between GrB and the observed high-elevation present day mass-balance field further validates the quality of the baseline model. As well, the improvement arising from the imposition of near-zero present-day net mass-balance lends some support to observational evidence that the whole Greenland ice-sheet is in a state of very near zero or weakly negative mass-balance.

6 CONCLUSIONS

By exploiting physically-based degrees of freedom to tune a glaciological reconstruction of the Greenland ice sheet, we have produced a dynamic ice-sheet model that provides a close match to the RSL record, to present day observed topography and to three GPS-based estimates of vertical bedrock displacement rates. With model tuning adjusted for near-zero present-day mass-balance, the regional pattern of surface mass-balance is also found to be in close correspondence with observations. In the eastern and western sectors, different RSL envelopes could be predicted by adjusting the calving parameterization, but the response to unloading generally lagged that suggested by the observational record. The only clear RSL discrepancy (Carey Island) is attributable to the topographic scale, local bathymetry, and lack of modelled ice shelves. The input topography only has deep bathymetry in the region and as such grounded ice is inhibited by the calving model.

Though we have shown significant sensitivity of the computed RSL histories to the model tuning, the methodology leaves open the question of the uniqueness of the tuning and thereby the extent of the constraint obtained on the resultant model of ice-sheet evolution. Furthermore, the set of constraints is by no means complete, witness the previously discussed discrepancy with the observed pattern of coastal to margin marine limit variation along the whole southwest coast. The geomorphology literature could provide an extremely useful complement to the RSL constraints employed in this study. The extent of climate tuning required also leaves open the question of what actual mix of dynamic processes were responsible for the strong Holocene margin variations that we were obliged to invoke in order to provide a match to the RSL record. The RSL data employed in this study is also lacking recent observations, especially high quality results from isolation basin studies. An up to date international database of carefully screened RSL records would certainly be of use.

In spite of these uncertainties, four primary conclusions appear to be warranted on the basis of this work. First, RSL constraints on ice-sheet thickness for observations near ice-sheet margins provide at most regional scale constraints. The ICE-4G reconstruction offers a reasonable match to RSL histories, but deglaciates about twice as much ice from Greenland as predicted by most of the available prognostic ice-sheet models. On the other hand, changes to local parameterizations for calving and the dependence of precipitation on temperature change had major impacts on computed RSL chronologies in certain regions, but had relatively minor impact on larger scale present day ice topography.

Secondly, a 120 km lithospheric thickness required significantly stronger forcing adjustments to the coupled model to match the RSL record. Though we cannot rule out such a lithospheric thickness, the requirement for excessive forcing does appear to favour the thinner lithosphere model. This is in accord with recent detailed reanalyses of the very extensive database of RSL histories for the British Isles (Peltier *et al.* 2002).

Thirdly, Greenland is dominated by widespread crustal subsidence except for regions in the north, northwest, and east. This is largely a signature of significant ice load increases during the mid-Holocene. Our final tuned model has an ice-sheet average rate of basal sinking of approximately 1.0 mm yr^{-1}. Even removing load variations for the last 1000 yr to remove more uncertain short-term ice load variations produces an average basal subsidence of 0.0 mm yr^{-1}. These values represent a significant departure from the 4 to 5 mm yr^{-1} uplift rates assumed in some current observational mass-balance studies (e.g. Krabill *et al.* 2000). Correcting assumed uplift rates would increase computed net mass-balance by about 10 km^3 yr^{-1}, reducing the inferred rate of mass loss from Greenland in the Krabill *et al.* (2000) analyses from 51 km^3 yr^{-1} to 41 km^3 yr^{-1}. This rate of mass loss corresponds to a contribution to the present day rate of global sea level rise of only 0.1 mm yr^{-1}. This is clearly not a significant part of the tide gauge inferred rate of global sea level rise of approximately 1.8 mm yr^{-1} (e.g. see Peltier 2001, for a recent discussion).

Finally, forward ice-sheet modelling combined with RSL history constraints provide a significant improvement in constraints on ice sheet reconstruction. Different scales of sensitivity ensure that RSL histories provide a non-trivial constraint on dynamic ice-sheet models. The small-scale aspects of calving, basal processes, and ice stream and outlet glacier dynamics leave considerable tuning degrees of freedom in current large-scale ice-sheet models as noted in Peltier (1994). Regional climatic uncertainties further de-constrain dynamic approaches. RSL histories on the other hand can provide strong complimentary local constraints on ice-sheet models. As a noteworthy example in this study, we were only able to match the outer envelope of the RSL data for Hall Land in north-northwestern Greenland by allowing complete glaciation of at least the central and northeastern parts of Nares strait between Greenland and Ellesmere Island.

Model GrB relies for its success on significant regional adjustments to the parameterizations for: calving, precipitation and Holocene surface temperatures. This clearly demonstrates the non-trivial nature of the imposition of RSL constraints on a dynamic ice-sheet model. Given model uncertainties, all of these adjustments can be motivated physically. A more internally-constrained approach to ice-sheet reconstruction must await incorporation of explicit ice stream/outlet glacier mechanics and better constrained climate forcings. An extension of the formalism with explicit ice-stream mechanics is in the process of development for the North American Wisconsin ice complex. This is much more complicated due to the lack of any constrained climate forcing history and to the much larger number of RSL observations available. For the present, the GrB model offers a RSL-constrained glaciologically-self-consistent deglaciation history that can act as a baseline for geophysical studies of Greenland and as boundary condition for atmospheric general circulation modelling. It will be incorporated into the ICE-5G successor to the ICE-4G global reconstruction of the last deglaciation event of the past ice-age.

REFERENCES

Bamber, J.L., Ekholm, S. & Krabill, W.S., 2001. A new, high-resolution digital elevation model of Greenland fully validated with airborne laser altimeter data, *J. geophys. Res.,* **106,** 6733–6745.

Blake, W.J., 1977. Radiocarbon age determinations from the Carey Islands, northwest Greenland, *Geolog. Serv. Can.,* **77-1A,** 445–454.

Braithwaite, R.J., 1995. Positive degree-day factors for ablation on the Greenland ice sheet studied by energy-balance modeling, *J. Glaciol.,* **41,** 153–160.

Calov, R. & Hutter, K., 1996. The thermomechanical response of the Greenland ice sheet to various climate scenarios, *Clim. Dyn.,* **12,** 243–260.

Cuffey, K.M., 2000. Methodology for use of isotopic climate forcings in ice sheet models, *Geophys. Res. Lett.,* **27,** 3065–3068.

Cuffey, K.M. & Clow, G.D., 1997. Temperature, accumulation and ice sheet elevation in central Greenland through the last deglacial transition, *J. geophys. Res.,* **102,** 26 383–26 396.

Cuffey, K.M. & Marshall, S.J., 2000. Substantial contribution to sea-level rise during the last interglacial from the Greenland ice sheet, *Nature,* **404,** 591–594.

Cuffey, K.M., Clow, G.D., Alley, R.B., Stuiver, M., Waddington, E.D. & Saltus, R.W., 1995. Large Arctic temperature change at the Wisconsin-Holocene glacial transition, *Science,* **270,** 455–458.

Cuffey, K.M., Conway, H., Gades, A., Hallet, B., Raymond, C.F. & Whitlow, S., 2000. Deformation properties of subfreezing glacier ice: Role of crystal size, chemical impurities, and rock particles inferred from in situ measurements, *J. geophys. Res.,* **105,** 27 895–27 915.

Dahl-Jensen, D. & Gundestrup, N.S., 1987. Constitutive properties of ice at Dye 3, Greenland, the physical basis of ice sheet modeling, *IAHS Publ.,* **170,** 31–43.

Dahl-Jensen, D., Mosegaard, K.N.G., Johnsen, G.D.C.S.J., Hansen, A.W. & Balling, N., 1998. Past temperatures directly from the Greenland ice sheet, *Science,* **282,** 268–271.

Dansgaard, W. *et al.*, 1993. Evidence for general instability of past climate from a 250 kyr ice-core record, *Nature,* **264,** 218–220.

Davis, C.H., Kluever, C.A. & Haines, B.J., 1998. Elevation change of the southern Greenland ice sheet, *Science,* **279,** 2086–2088.

DeLaughter, J., Stein, S. & Stein, C.A., 1999. Extraction of a lithospheric cooling signal from ocean-wide geoid data, *Earth planet. Sci. Lett.,* **174,** 173–181.

Dziewonski, A.M. & Anderson, D.L., 1981. Preliminary reference Earth model, *Phys. Earth planet. Inter.,* **25,** 297–356.

Echelmeyer, K., Clarke, T.Z. & Harrison, W.D., 1991. Surficial glaciology of Jakobshavns Isbrae, West Greenland: Part i. surface morphology, *J. Glaciol.,* **37,** 368–382.

England, J., 1976. Late Quaternary glaciation of the northeastern Queen Elizabeth Islands, N. W. T., Canada: alternative models, *Quat. Res.,* **6,** 185–202.

England, J., 1985. The late Quaternary history of Hall Land, NW Greenland, *Can. J. Earth Sci.,* **22,** 1394–1408.

England, J., 1999. Coalescent Greenland and Innuitian ice during the Last Glacial Maximum: revising the Quaternary of the Canadian High Arctic, *Quat. Sci. Rev.,* **18,** 421–456.

Fawcett, P.J., Agustsdottir, A.M., Alley, R.B., Funder, C.A.S.S. & Hansen, L., 1997. The Younger Dryas termination and North Atlantic Deep Water formation: Insights from climate model simulations and Greenland ice cores, *Paleoc,* **12,** 23–38.

Funder, S. & Hansen, L., 1996. The Greenland ice sheet—a model for its culmination and decay during and after the last glacial maximum, *Bull. geol. Soc. of Denmark,* **42,** 137–152.

Funder, S., Hjort, C., Landvik, J.Y., Nam, S., Reeh, N. & Stein, R., 1998. History of a stable ice margin: East Greenland during the Middle and Upper Pleistocene, *Quat. Sci. Rev.,* **17,** 77–123.

Goldsby, D.L. & Kohlstedt, D.L., 1997. Grain boundary sliding in fine-grained ice I, *Scr. Mater.,* **37,** 1399–1406.

Greve, R., 2000. On the response of the Greenland ice sheet to greenhouse climate change, *Clim. Change,* **46,** 289–303.

Greve, R., Weis, M. & Hutter, K., 1998. Palaeoclimatic evolution and present conditions of the Greenland ice sheet in the vicinity of Summit: An approach by large-scale modelling, *Palaeoclim., Data and Model.,* **2,** 133–162.

Hindmarsh, R.C. & Payne, A.J., 1996. Time-step limits for stable solutions of the ice sheet equation, *Ann. Glaciol.,* **23,** 74–85.

Huybrechts, P., 1996. Basal temperature conditions of the Greenland ice sheet during the glacial cycle, *Ann. Glaciol.,* **23,** 226–236.

Huybrechts, P., 2002. Sea-level changes at the LGM from ice-dynamic reconstructions of the Greenland and Antarctic ice sheets during the glacial cycles, *Quat. Sci. Rev.,* **21,** 203–231.

Huybrechts, P. & de Wolde, J., 1999. The dynamic response of the Greenland and Antarctic ice sheets to multiple-century climatic warming, *J. Climate,* **12,** 2169–2188.

Huybrechts, P., Letreguilly, A. & Reeh, N., 1991. The Greenland ice sheet and greenhouse warming, *Palaeogeogr., Palaeoclimato., Palaeoecol.,* **89,** 399–412.

Jacka, T.H. & Jun, L., 1994. The steady-state crystal size of deforming ice, *Ann. Glaciol.,* **20,** 13–18.

Janssens, I. & Huybrechts, P., 2000. The treatment of meltwater retention in mass-balance parameterizations of the Greenland ice sheet, *Ann. Glaciol.,* **31,** 14–23.

Johnsen, S.J., Dansgaard, W. & White, J.W.C., 1989. The origin of Arctic precipitation under present and glacial conditions, *Tellus,* **41,** 452–469.

Kelly, M., Funder, S., Houmark-nielsen, M., Knudsen, K.L., Kronborg, C., Landvik, J. & Sorby, L., 1999. Quaternary glacial and marine environemental history of northwest Greenland: a review and reappraisal, *Quat. Sci. Rev.,* **18,** 373–392.

Kincaid, D.R., Oppe, T.C. & Joubert, W.D., 1989. An overview of NSPCG: A nonsymmetric preconditioned conjugate gradient package, in *Practical Iterative Methods for Large Scale Computations,* pp. 283–293, eds Boley, L., Truhlar, D.G., Saad, Y., Wyatt, R.E. & Collins, L.A., North-Holland, Amsterdam.

Krabill, W. *et al.*, 2000. Greenland ice sheet: High-elevation balance and peripheral thinning, *Science,* **428–430**.

Kutzbach, J.E. & Guetter, P.J., 1986. The influence of changing orbital parameters and surface boundary conditions on climate simulations for the past 18000 years, *J. Atmos. Sci.,* **43,** 1726–1759.

Lambeck, K., Smither, C. & Johnston, P., 1998. Sea level change, glacial rebound and mantle viscosity for northern Europe, *Geophys. J. Int.,* **134,** 102–144.

Lasca, N.P., 1966. Post-glacial delevelling in Skeldal, northeast Greenland, *Arctic,* **19,** 349–353.

Legates, D.R. & Willmott, C.J., 1990. Mean seasonal and spatial variability in gauge-corrected global precipitation, *Int. J. Climatol.,* **10,** 111–127.

Le Meur, E. & Huybrechts, P., 1996. A comparison of different ways of dealing with isostasy: examples form modelling the Antarctic ice sheet during the last glacial cycle, *Ann. Glaciol.,* **23,** 309–317.

Letreguilly, A., Huybrechts, P. & Reeh, N., 1991. Steady-state characteristics of the Greenland ice sheet under different climates, *J. Glaciol.,* **37,** 149–157.

Montagnat, M. & Duval, P., 2000. Rate controlling processes in the creep of polar ice, influence of grain boundary migration associated with recrystallization, *Earth planet. Sci. Lett.,* **183,** 179–186.

Oerlemans, J., 1991. The mass balance of the Greenland ice sheet: sensitivity to climate change as revealed by energy-balance modelling, *Holocene,* **1,** 40–49.

Ohmura, A. & Reeh, N., 1991. New precipitation and accumulation maps for Greenland, *J. Glaciol.,* **37,** 140–148.

Ohmura, A., Calanca, P., Wild, M. & Anklin, M., 1991. Precipitation, accumulation and mass balance of the Greenland ice sheet, *Z. Gletscherkd. Glazialgeol.,* **35,** 1–20.

Parsons, B. & Sclater, J.G., 1977. An analysis of the variation of ocean floor bathymetry and heat flow with age, *J. geophys. Res.,* **82,** 803–827.

Patankar, S.V., 1980. *Numerical Heat Transfer and Fluid Flow,* Hemisphere, New York.

Paterson, W.S.B., 1991. Why ice-age ice is sometimes 'soft', *Cold Reg. Sci. Tech.,* **20,** 75–98.

Paterson, W.S.B., 1994. *The Physics of Glaciers,* Pergamon, Tarrytown.

Payne, A.J. & Dongelmans, P.W., 1997. Self-organization in the thermomechanical flow of ice sheets, *J. geophys. Res.,* **102,** 12 219–12 234.

Payne, A.J. & others, 2000. Results from the EISMINT model intercomparison: the effects of thermomechanical coupling, *J. Glaciol.,* **46,** 227–238.

Peltier, W.R., 1974. The impulse response of a Maxwell Earth, *Rev. Geophys.,* **12,** 649–669.

Peltier, W.R., 1976. Glacial isostatic adjustment ii: the inverse problem, *Geophys. J. R. astr. Soc.,* **46,** 669–706.

Peltier, W.R., 1994. Ice age paleotopography, *Science,* **265,** 195–201.

Peltier, W.R., 1996. Mantle viscosity and ice age ice sheet topography, *Science,* **273,** 1359–1364.

Peltier, W.R., 1998. Postglacial variations in the level of the sea: implications for climate dynamics and solid-earth geophysics, *Rev. Geophys.,* **36,** 603–689.

Peltier, W.R., 1999. Global sea level rise and glacial isostatic adjustment, *Glob. Plan. Change,* **20,** 93–123.

Peltier, W.R., 2001. Global glacial isostatic adjustment and modern instrumental records of relative sea level history, in *Sea Level Rise: History and Consequences,* pp. 65–95, eds Douglas, B.C., Kearney, M.S. & Leatherman, S.P., Acad. Press, San Diego.

Peltier, W.R. & Jiang, X., 1996. Mantle viscosity from the simultaneous inversion of multiple data sets pertaining to postglacial rebound, *Geophys. Res. Lett.,* **23,** 503–506.

Peltier, W.R., Goldsby, D.L., Kohlstedt, D.L. & Tarasov, L., 2000. Ice-age ice-sheet rheology: constraints from Last Glacial Maximum form of the Laurentide ice sheet, *Ann. Glaciol.,* **30,** 163–176.

Peltier, W.R., Shennan, I., Drummond, R. & Horton, B., 2002. On the postglacial isostatic adjustment of the British Isles and the shallow viscoelastic structure of the Earth, *Geophys. J. Int.,* **148,** 443–475.

Pfeffer, W.T., Meier, M.F. & Illangasekare, T.H., 1991. Retention of Greenland runoff by refreezing: implications for projected future sea level change, *J. geophys. Res.,* **96,** 22 117–22 224.

Pinot, S., Ramstein, G., Harrisen, S.P., Prentice, I.G., Guiot, J., Stute, M. & Joussaume, S., 1999. Tropical paleoclimates at the last Glacial Maximum: Comparison of Paleoclimate Modeling Intercomparison (PMIP) simulations and paleodata, *Clim. Dyn.,* **15,** 857–874.

Rasch, 1997. A compilation of radiocarbon dates from Disko Bugt, central West Greenland, *Dan. J. Geogr.,* **97,** 143–151.

Rasch, M., 2000. Holocene relative sea level changes in Disko Bugt, West Greenland, *J coast. Res.,* **16,** 306–315.

Rasch, M. & Nielsen, N., 1995. Coastal morpho-stratigraphy and Holocene relative sea level changes at Tuapaat, southeastern Disko Island, central West Greenland, *Polar Res., 14,* 277–289.

Reeh, N., 1989. Parameterization of melt rate and surface temperature on the Greenland ice sheet, *Polarforschung, 59,* 113–128.

Ritz, C., Fabre, A. & Letreguilly, A., 1997. Sensitivity of a Greenland ice sheet model to ice flow and ablation parameters: Consequences for evolution through the last climatic cycle, *Clim. Dyn., 13,* 11–24.

Ritz, C., Rommelaere, V. & Dumas, C., 2001. Modeling the evolution of Antarctic ice sheet over the last 420,000 years: implications for altitude changes in the Vostok region, *J. geophys. Res., 106,* 31 943–31 964.

Schaeffer, F.R.P., & Legresy, B., 1999. Ice flow processes derived from ERS-1 high-resolution map of Antarctica and Greenland ice sheet, *Geophys. J. Int., 139,* 645–656.

Severinghaus, J.P., Sowers, T., Brook, E.J., Alley, R.B. & Bender, M.L., 1998. Timing of abrupt climate change at the end of the Younger Dryas interval from thermally fractionated gases in polar ice, *Nature, 391,* 141–146.

Shennan, I., Lambeck, K., Horton, B.P., Innes, J.B., Lloyd, J.M., McArthur, J.J., Purcell, T. & Rutherford, M.M., 2000. Late Devensian and Holocene records of relative sea-level changes in northwest Scotland and their implications for glacio-hydro-isostatic modelling, *Quat. Sci. Rev., 19,* 1103–1136.

Shottont, F.W. & Williams, R.E.G., 1974. Birmingham University radiocarbon dates, *Radiocarbon, 16,* 285–303.

Stuiver, M. & Reimer, P.J., 1993. Extended ^{14}C database and revised CALIB radiocarbon calibration program, *Radiocarbon, 35,* 215–230.

Stuiver, M., Reimer, P.J. & Braziunas, T.F., 1998. High-precision radiocarbon age calibration for terrestrial and marine samples, *Radiocarbon, 40,* 1127–1151.

Tarasov, L. & Peltier, W.R., 1997a. Terminating the 100 kyr ice age cycle, *J. geophys. Res., 102,* 21 665–21 693.

Tarasov, L. & Peltier, W.R., 1997b. A high-resolution model of the 100 kyr ice age cycle, *Ann. Glaciol., 25,* 58–65.

Tarasov, L. & Peltier, W.R., 1999. Impact of thermomechanical ice sheet coupling on a model of the 100 kyr ice age cycle, *J. geophys. Res., 104,* 9517–9545.

Tarasov, L. & Peltier, W.R., 2002. Greenland glacial history, borehole constraints and Eemian extent, *J. geophys. Res.,* in press.

Ten Brink, N.W. & Weidick, A., 1974. Greenland ice sheet history since the last glaciation, *Quat. Res., 4,* 429–440.

Thomas, R., Akins, T., Csatho, B., Fhanestock, M., Gogineni, P., Kim, C. & Sonntag, J., 2000. Mass balance of the Greenland ice sheet at high elevations, *Science, 289,* 426–428.

Thorsteinsson, T., Waddington, D.E., Taylor, C.K., Alley, B.R. & Blankenship, D.D., 1999. Strain rate enhancement at Dye 3, Greenland, *J. Glaciol., 45,* 338–345.

Trautman, M.A. & Willis, E.H., 1963. Isotopes, Inc., radiocarbon measurements iii, *Radiocarbon, 5,* 62–79.

Tushingham, A.M. & Peltier, W.R., 1991. ICE-3G: a new global model of late-Pleistocene deglaciation based upon geophysical predictions of post-glacial relative sea-level changes, *J. geophys. Res., 96,* 4497–4523.

Tushingham, A.M. & Peltier, W.R., 1992. Validation of the ICE-3G model of Wurm-Wisconsin deglaciation using a global data base of relative sea level histories, *J. geophys. Res., 97,* 3285–3304.

Van de Wal, R., 1996. Mass-balance modelling of the Greenland ice sheet: a comparison of an energy-balance and a degree-day model, *Ann. Glaciol., 23,* 36–45.

Van Tatenhove, F.G., Fabre, A., Greve, R. & Huybrechts, P., 1996. Modelled ice-sheet margins of three Greenland ice-sheet models compared with a geological record from ice-marginal deposits in central West Greenland, *Ann. Glaciol., 23,* 52–58.

Vettoretti, G., Peltier, W.R. & McFarlane, N.A., 2000a. The simulated response of the climate system to soil moisture perturbations under paleo-climatic boundary conditions at 6000 years before present, *Can. J. Earth Sci., 37,* 635–660.

Vettoretti, G., Peltier, W.R. & McFarlane, N.A., 2000b. Global balance and atmospheric water vapour transport at Last Glacial Maximum: Climate simulations with the CCCma atmospheric general circulation model, *Can. J. Earth Sci., 7,* 695–723.

Wahr, J., van Dam, T. & Francis, O., 2001. Geodetic measurements in Greenland and their implications, *J. geophys. Res., 106,* 16 567–16 581.

Wahr, J., van Dam, T., Larson, K. & Francis, O., 2002. GPS measurements of vertical crustal motion in Greenland, *J. geophys. Res., 106,* 33 755–33 760.

Washburn, A.L. & Stuiver, M., 1962. Radiocarbon-dated post-glacial deleveling in northeast Greenland and its implications, *Arctic, 15,* 66–73.

Weidick, A., 1972a. Holocene shorelines and glacial stages in Greenland, Tech. Rep. 41, Gronlands Geol. Unders.

Weidick, A., 1972b. C14 dating of survey material performed in 1971, Tech. Rep. 45, Gronlands Geol. Unders.

Weidick, A., 1993. Neoglacial change of ice cover and the related response of the Earth's crust in west Greenland, Tech. Rep. 41, Gronlands Geol. Unders.

Weidick, A., Oerter, H., Reeh, N., Thomsen, H.H. & Thorning, L., 1990. The recession of the inland ice margin during the Holocene climatic optimum in the Jakobshavn Isfjord area of west Greenland, *Palaeog., Palaeocl., Palaeoeco., 82,* 389–399.

White, J.W.C., Barlow, L.K., Fisher, D., Grootes, P., Jouzel, J., Johnsen, S.J., Stuiver, M. & Clausen, H., 1997. The climate signal in the stable isotopes of Summit, Greenland: Results of comparisons with modern climate observations, *J. geophys. Res., 102,* 26 425–26 439.

World Data Center-A for Paleoclimatology, National Geophysical Data Center, B., 1997. The Greenland Summit Ice Cores CD-ROM, CD-ROM.

Wu, P. & Peltier, W.R., 1982. Viscous gravitational relaxation, *Geophys. J. R. astr. Soc., 70,* 435–485.

Zreda, M.J.E., Phillips, F., Elmore, D. & Sharma, P., 1999. Unblocking of the Nares Strait by Greenland and Ellesmere ice-sheet retreat 10 000 years ago, *Nature, 398,* 139–142.

APPENDIX: REGIONAL HOLOCENE TEMPERATURE ADJUSTMENT

The regional Holocene temperature adjustment ΔT_{adj} is given by

$$\Delta T_{\mathrm{adj}} = T_{\mathrm{adjB}} * (12000\ \mathrm{m} - h)/12000\ \mathrm{m} \tag{A1}$$

with

$$T_{\mathrm{adjB}} = \begin{cases} 0 & t_e > t \\ T_h * 0.8 * (t - t_e)/(t_h - t_e) & t_h > t \geq t_e \\ T_h & -8\ \mathrm{kyr} > t \geq t_h \\ T_h + (T_l - T_h) * (t - t_h)/(t_l + 8\ \mathrm{kyr}) & t_l > t \geq -8\ \mathrm{kyr} \\ T_l & t \geq t_l \end{cases} \tag{A2}$$

and with variable values given in Table A1.

Table A1. Regional surface temperature modification key for use in eq. (A2).

Region	T_h	Longitude	Latitude (N)	t_e	t_h	t_l	T_l
Disko	7.0	W → 46W	71 → 69	−10.5 kyr	−9 kyr	−5 kyr	2.5
Sondre	10.0	W → 46W	69 → 65	−11.0 kyr	−10.0 kyr	−7 kyr	−2.0
Kapisigdlit	6.0	W → 46W	65 → 63.5	−10.5 kyr	−9 kyr	−5 kyr	0.6
Nerutussoq	10.0	W → 46W	63.5 → 59	−10.5 kyr	−9 kyr	−5 kyr	3.2
East	9.0	32W → E	75 → 69	−11 kyr	−9.5 kyr	−7 kyr	0.1
Hall Land	3.0	61W → 45W	82 → 79	−10.5 kyr	−9 kyr	−6 kyr	0.0